The pH-dependent processivity of Arabidopsis AtPME2 can control cell wall mechanical properties

Ludivine Hocq[1§], Olivier Habrylo[1¥], Aline Voxeur[1#], Corinne Pau-Roblot[1], Josip Safran[1], Fabien Sénéchal[1], Françoise Fournet[1], Solène Bassard[1], Virginie Battu[2], Hervé Demailly[3], José C. Tovar[4†], Serge Pilard[5], Paulo Marcelo[6], Brett J. Savary[4], Davide Mercadante[7], Maria Fransiska Njo[8,9], Tom Beeckman[8,9], Arezki Boudaoud[2], Jérôme Pelloux[1]*, Valérie Lefebvre[1]*

[1] : UMRT INRAE 1158 BioEcoAgro – BIOPI Biologie des Plantes et Innovation, SFR Condorcet FR CNRS 3417, Université de Picardie, 33 Rue St Leu, 80039 Amiens, France. [2] : Laboratoire Reproduction et Développement des Plantes, UMR 5667, ENS de Lyon, BP 7000 69342 Lyon Cedex 07 France. [3.] : CRRBM, Université de Picardie, 33 Rue St Leu, 80039 Amiens, France. [4.] : Arkansas Biosciences Institute, Arkansas State University, Jonesboro, AR 72467, USA.[5] : Plateforme Analytique, Université de Picardie, 33 Rue St Leu, 80039 Amiens, France. [6] : Plateforme d'Ingénierie cellulaire et d'Analyses des Protéines, CURS, Avenue Laënnec - 80054 Amiens cedex 1, Université de Picardie. [7]: School of Chemical Sciences, The University of Auckland, Private Bag 92019, Auckland 1142, New Zealand. [8]: Ghent University, Department of Plant Biotechnology and Bioinformatics, 9052 Ghent, Belgium. [9]: VIB Center for Plant Systems Biology, 9052 Ghent, Belgium.

[§] Present address : UMR1121 Laboratoire Agronomie et Environnement, Université de Lorraine – INRAE, 2 Avenue de la Forêt de Haye, 54505 Vandoeuvre les Nancy, France

[¥] Present address: Centre de Recherche et Innovation Soufflet, 1 rue de la Poterne à Sel, 10400 Nogent sur Seine, France

[#] Present address: INRAE, Institut Jean-Pierre Bourgin, UMR1318 INRAE-AgroParisTech, ERL3559 CNRS, Saclay Plant Sciences, 78026 Versailles, France

[†] Present address: Donald Danforth Plant Science Center, 975 N. Warson Rd., St. Louis, MO 63132, USA

*: contributed equally to the work as senior authors.

Corresponding author:

J.P and V.L.: EA3900-BIOPI, Université de Picardie Jules Verne, Amiens, France.

jerome.pelloux@u-picardie.fr

valerie.lefebvre@u-picardie.fr

Running title:

AtPME2 has a pH-dependent processivity

Abstract (195 Words)

Pectin methylesterases (PMEs) modify homogalacturonan's chemistry and thereby play a key role in regulating primary cell wall mechanical properties. How PME activity can fine-tune pectin structure in the growing plant has remained elusive, in part due to the lack of available biochemically-characterized enzymes to empirically test functional properties. Here we report on AtPME2, which we found to be highly expressed during lateral root emergence as well as root and hypocotyl elongation. Production of mature active enzyme in *Pichia pastoris* allowed its biochemical characterization. We show that AtPME2 can switch from full processivity (at pH 8), creating large blocks of unmethylated galacturonic acid, to low processivity (at pH 5) and relate these observations to the differences in electrostatic potential of the protein. We also produced a generic plant PME antiserum suitable for detecting recombinant and native enzyme independent of species source. In the context of acidified apoplast, we showed using reverse genetics that low-processive demethylesterification by AtPME2 can loosen the cell wall, with consequent increase in cell elongation and etiolated hypocotyl length. Our study brings insights into how the pH-dependent regulation by PME activity could affect pectin structure and associated cell wall mechanical properties in expansion.

Introduction

How plants control pectin's chemistry in cell walls is a central question in plant growth and development and in plant response to abiotic and biotic stresses. Pectins are complex polysaccharides that function as key structural elements regulating the mechanical properties of plant cell walls. Pectins are enriched in galacturonic acid and comprise four main domains: homogalacturonan (HG), rhamnogalacturonan-I (RG-I), rhamnogalacturonan-II (RG-II) and xylogalacturonan (XG). One key feature of HG chemistry, a homopolymer of α-1,4-linked-D-galacturonic acid units, is the presence of methyl- and acetyl-ester substitutions along the polymer chain that modify its physical, chemical, and biochemical properties (Ridley *et al.*, 2001). Plants synthesize HG as a highly methylesterified form (up to 80% methyl esters, occurring at the C-6 carboxyl position) and a low acetylated form (up to 5-10% acetyl ester, occurring at the O-2 or O-3 positions) in the Golgi apparatus, before being exported to the apoplastic space. The degree of methylesterification (DM) and degree of acetylation (DA) as well as distribution of these substitutions on the backbone are fine-tuned at the cell wall by pectin methylesterases (PMEs, EC 3.1.1.11) and pectin acetylesterases (PAE, EC 3.1.1.6), respectively (Pelloux *et al.*, 2007). Pectin methylesterase action on HG is tightly regulated biochemically by proteinaceous inhibitors called pectin methylesterase inhibitors (PMEIs) or by pH and cations (Micheli, 2001). Resulting activity can introduce extensive de-methylesterified HG blocks that can bind Ca^{2+} ions cooperatively, creating so called "egg-box" cross-link structures that promote cell wall rigidity (Willats *et al.*, 2006). Limited de-methylesterified blocks may also provide substrate-binding sites for pectin-depolymerizing enzymes such as polygalacturonases (endo-PGs, EC 3.2.1.15) and pectin/pectate lyases-like (PLLs EC 4.2.2.2), which reduce HG's degree of polymerization (DP) and promotes the pectic network's deconstruction (Sénéchal, Wattier, *et al.*, 2014). Therefore, to relate the consequences of PME action on pectin substrates to changes in the cell wall's elasticity, it is key to determine their degree of processivity (*i.e.*, the extent PME hydrolyzes consecutive methylesters).

Plants are well described for expressing multiple PME isoforms with individual isozymes varying in tissue-specific expression patterns, biochemical properties, and action patterns. PMEs thereby likely function differentially in the cell wall during plant growth and development (Goldberg *et al.*, 1996; Micheli, 2001; Pelloux *et al.*, 2007). PMEs were indeed reported to play a key role in developmental processes as diverse as hypocotyl elongation (Pelletier *et al.*, 2010), pollen tube growth (Leroux *et al.*, 2015), root development (Hewezi *et*

al., 2008), organogenesis at the shoot apical meristem (Peaucelle *et al.*, 2008; Peaucelle *et al.*, 2011), and gynoeceum development (Andres-Robin *et al.*, 2018). Contradictory reports showed that PME activity can either induce cell wall stiffening or loosening, with distinct consequences on plant development (Peaucelle *et al.*, 2015; Daher *et al.*, 2018; Wang *et al.*, 2020). This could at least partly be explained by the demethylation pattern that different PME isoforms would create in relation to their processivity which could be regulated by the local cell wall microenvironment, including ion concentrations, apoplastic pH, enzyme's localization, and presence of inhibitory proteins.

Because plant PMEs are encoded by large multigenic family (e.g., 66 genes in Arabidopsis; Sénéchal, Wattier, *et al.*, 2014), there is need to determine the expression profile and degree of processivity of individual isoforms to assess their potential for generating HG micro-domains that differ in de-methylesterified block sizes. Such micro-domains were recently reported to play a key role in determining the control of mucilage release in Arabidopsis seeds through interaction with peroxidases (Francoz *et al.*, 2019). Plant PMEs typically have neutral to alkaline pH activity optimum (Jolie *et al.*, 2010; Dixit *et al.*, 2013) although few acidic isoforms are reported (Lin *et al.*, 1989; Thonar *et al.*, 2006). It is generally recognized that plant and microbial PMEs differ in their processivity. Plant and bacterial PMEs produce large blocks of demethylesterified HG by processive action, while fungal enzymes act more randomly on their substrate to provide single or limited consecutive demethylesterifications (Mercadante *et al.*, 2013; Mercadante *et al.*, 2014; Sénéchal *et al.*, 2015; Kent *et al.*, 2016; Fries *et al.*, 2007). The structural determinants for differences in processivity were determined (Mercadante *et al.*, 2014; Kent *et al.*, 2016), with key suggestions about the role of charged residues in certain subsites of the enzyme binding groove, and the interplay of electrostatic *versus* hydrophobic contacts in favoring substrate-binding and sliding along the groove to achieve processivity (Mercadante *et al.*, 2014; Kent *et al.*, 2016; Fries *et al.*, 2007). The myriad of PME isoforms expressed in plants is however suggestive of a very fine regulation of the processive activity. The binding of certain methylation pattern and the enzymatic release after a certain number of de-methylesterification cycles are likely to be fine-tuned to modulate the physico-chemical properties of plant cell wall pectin in accordance to the micro-environment. PME processivity of an apple PME was shown to be pH-dependent, with a possible shift from a blockwise to non-blockwise mode of action (Denès *et al.*, 2000), and processive fungal PMEs were also reported (Markovič and Kohn, 1984). Considering such complexity of the PMEs' landscape, it is therefore paramount to adopt a more comprehensive approach in which biochemical data

are combined with structural and biophysical information of PMEs activity. Nevertheless, studying the crystal structure or mode of action of rare plant PMEs (i.e., low abundant proteins due to limited temporal and tissue-specific expression) has been impaired by the ability to produce purified native enzyme in quantities sufficient for refined structural studies. Routine heterologous expression of effectively folded plant PMEs has been challenging, thus their precise mode of action remains unresolved (Cheong *et al.*, 2019).

In higher plants, PMEs harbor two distinct protein structures: group 1 PMEs (21 isoforms in Arabidopsis) that contain a mature active part (PME catalytic domain, Pfam01095) that can be preceded by a signal peptide or a transmembrane domain (Sénéchal, Wattier, *et al.*, 2014; Pelloux *et al.*, 2007; Markovič and Janeček, 2004), while group 2 PMEs (45 isoforms in Arabidopsis) have, in addition to the catalytic part, an N-terminal extension (PRO-domain) showing sequence similarities with the PMEI domain (Pfam04043), in addition to the catalytic domain.

We describe here for the first time that Arabidopsis *AtPME2* (At1g53830), encoding a group 2 PME is strongly expressed in dark-grown hypocotyls and roots, and that the protein localizes at the cell wall. We successfully expressed active AtPME2 in the yeast *Pichia pastoris*, and using generic PME antibodies generated from a designed peptide immunogen, we show that the PRO-part is important for processing the enzyme into its mature active form. We further determined that AtPME2 is more active on moderately to highly methylesterified pectic substrates, with a high processivity at neutral pH, while it shows a low degree of processivity in acidic conditions. And finally, using loss-of-function mutant plants for *AtPME2*, we showed that the enzyme may play a key role in controlling dark-grown hypocotyl development through modulating the cell wall's structural chemistry and mechanics. This study brings insights on how the differential expression of an individual Arabidopsis PME isoform having distinctive processivity for homogalacturonan may contribute to structural changes in the cell wall that affect plant development.

Results

AtPME2 gene is expressed in dark-grown hypocotyls and roots

AtPME2 (At1g53830) gene expression was followed using RT-qPCR transcript profiling in various organs (roots, dark-grown hypocotyls, leaves, stem, siliques, floral buds and seeds) and was found highly expressed in dark-grown hypocotyls and roots as compared to leaves, stem, floral buds and seeds. In contrast, no expression was detected in siliques (**Figure 1A**). During the time course of dark-grown hypocotyl development, an increase in *AtPME2* transcripts was measured up to 72 h post-induction (**Figure 1B**). This timing corresponds to the acceleration phase of growth according to previously published work (Pelletier *et al.*, 2010). In contrast, *AtPME2* was stably expressed in roots during seedling development in the light (**data not shown**).

AtPME2 promoter activity was further localized using a *GUS* reporter gene. Following plant transformation, GUS staining was assessed in light-grown and 4 day-old dark-grown seedlings. In etiolated hypocotyls, the promoter activity was mainly localized in the upper part of the organ (**Figure 1C, left panel**). During lateral root formation, no GUS staining was detected in the early stages (stages I to V) of primordia differenciation, while a strong signal was observed at later stages (from VI onwards) (**Figure 1C, upper panel**). In elongating roots (either primary, lateral or adventitious), *AtPME2* promoter activity was mainly present in the elongation zone (**Figure 1C, lower panel**).

AtPME2 protein is present as a processed isoform in the cell wall

Using proteomic profiling, we identified the pectin remodeling enzymes PME, PAE, PG, PLL and the regulatory proteins PMEI and SBT (subtilase) in cell wall-enriched protein fractions isolated from either 4-day-old hypocotyls (**Supplemental Table IA**) and 7-day-old roots (**Supplemental Table IB**), of Col-0 and WS ecotypes. In hypocotyls, these include AtPME2 (AT1G53830) and two additional PME isoforms (AT3G14310, AT4G33220), as well as multiple PMEI proteins (AT2G43050; AT4G25260…), PAEs (AT2G46930, AT3G05910, AT5G45280…), PLLs (AT3G06770, AT3G07010, AT3G55140…) and SBTs (AT1G01900, AT1G20160, AT5G51750…) in both Col-0 and WS. Interestingly, some proteins were specifically identified in only one of the ecotypes (e.g., AT3G07010 in Col-0 and AT3G09410, AT3G59010, AT5G20740, AT5G46960, AT5G62350 in WS). PME, PAE, PMEI, PLL were identified in cell wall-enriched protein fractions of roots, but with some enzymes expressed only in one ecotype or the other. While some proteins (e.g., AT3G14310,

AT4G19410, AT3G16850…) were common with those identified in hypocotyls, others appeared to be specific to roots (e.g. AT1G32940, AT2G45220, AT4G34980…). Depending on the ecotype, the proteomic analysis matched 4 or 5 peptides predicted in the PME catalytic domain, accounting for 19% sequence coverage for AtPME2 (**Supplemental Figure 1 and Supplemental Table IA, B**). This survey confirmed that AtPME2 was indeed present in cell wall-enriched protein fractions of both organs, thus supporting transcriptional data. No peptides mapping to the PRO-domain were detected, consistent with AtPME2 being processed before export to the apoplast.

To further verify the secretion of AtPME2 in the apoplasm, we designed a genetic construct tagging AtPME2 with GFP attached at the C-terminus of the mature protein sequence. Following plant transformation, confocal imaging of plasmolyzed root cells revealed GFP fluorescence was detected at both the cell wall and in the cytoplasm (**Figure 1E**). This is consistent with AtPME2 translocation to the cell wall where it acts to fine-tune pectin structure and with previous reports relating nascent protein processing to the mature protein during transport in Golgi vesicles (Micheli, 2001).

AtPME2 can be effectively produced and processed as an active isoform in *Pichia pastoris*

To produce pure active enzyme for biochemical studies, we first attempted to directly express the catalytic domain without the PRO-peptide (PMEI-like domain) in *Pichia pastoris*. We amplified the putative coding sequence for the mature part, starting from KADA, downstream the second putative processing motif (RLLL, reported to be cleaved by the action of subtilisin-like proteases, removing the PRO regions and releasing active enzymes at the cell wall (Wolf et al., 2009)), up to the end of the sequence minus the stop codon (**Supplemental Figure 2B**, referred as "MAT" construct). This construct was cloned in frame with 6xHIS tag into the pPICZ αB yeast expression vector, harboring a fungal secretory peptide. Following Pichia transformation, selection, and induction of transformants, we failed to detect any PME activity in concentrated supernatants. Considering the hypothesis that the PMEI domain functions as a chaperone during PME transport and processing (Micheli, 2001), we next inserted the full length AtPME2 coding sequence into the above-mentioned pPICZ αB vector, including its PRO-domain (but minus the plant secretory signal peptide and STOP codon, referred as "FL" construct, from ATTT to SLSL amino acids, **Supplemental Figure 2A and 2B**) and transformed *Pichia pastoris*. PME activity was this time detected in concentrated supernatants of induced transformants. While we were unable to recover PME

activity after polyhistidine-tag affinity purification (presumably due to degradation of the affinity tag), we used cation exchange chromatography to purify the recombinant AtPME2, which is shown by SDS-PAGE (Coomassie-Blue stained gel) in **Figure 2A**. One band is present at ~30 kDa and two bands are observed at ~35 kDa, the latter corresponding to the approximate mass calculated from the sequence for the mature AtPME2 protein. The doublet is consistent with AtPME2 being cleaved at either of the processing motifs (RKLK and RRLL, see **Supplemental Figure 1 and 2B**) by *Pichia pastoris* subtilisin protease. The identity of AtPME2 mature protein was confirmed by mass spectrometry of the tryptic peptides, matching 12 peptides (**Supplemental Figure 3**). The lower protein, ~30 kDa, corresponds to the PRO-peptide, which was confirmed by matching 7 tryptic peptides (**Supplemental Figure 3**). Using the Pichia expression system, we were thus able to produce the mature active AtPME2 enzyme, as well as recover the PRO-peptide.

To support detection and identification of plant PMEs such as AtPME2 in expression studies, we produced an antiserum that could be broadly selective for plant PMEs (*i.e.*, generic for plants, independent of species source) in western blotting. For this we synthesized a peptide immunogen using a 15 amino acid peptide sequence (KTYLGRPWKEYSRTV) that spans the highly conserved region V in plant PMEs and includes two invariant residues participating in the enzyme's catalytic site (Markovič and Janeček, 2004). Sequences alignment of 45 Arabidopsis PME catalytic domains (**Supplemental Figure 4A**) showed that this amino acid sequence is indeed highly conserved, notably in AtPME2 (AT1G53830, PTYLGRPWKEYSRTV) and AtPME3 (AT3G14310, PTYLGRPWKEYS**Q**TV) sequences, two of the proteins identified both in hypocotyls and roots in our proteomic analyses. Western blot analyses to assess this generic PME antibody first examined previously purified PME isoforms isolated from citrus (CsTT-PME, CsPME2 and CsPME4) and tomato (SlPME1) fruit (Savary, 2001; Savary *et al.*, 2010; Savary *et al.*, 2013). The strong antiserum binding signal (dilution at 1:3000) indicates high affinity for all four PMEs (**Figure 2B**). We similarly tested the antiserum against previously purified AtPME3 (Sénéchal *et al.*, 2015), which also showed strong binding (**Supplemental Figure 4B**), thus supporting the generic antiserum provides a new tool for analyzing Arabidopsis PMEs.

To assess this generic antiserum's sensitivity for detecting PMEs present in cell wall-enriched protein fractions, we performed western-bot analysis using Arabidopsis hypocotyl and root extracts. We detected antigen signals at approximately 35 kDa, which is consistent with the predicted size of fully processed (mature) PME (**Figure 2C**). Additional bands were detected above ~55 kDa, which may represent unprocessed PME precursor proteins isolated

from plant tissue extracts. No antigen signal was detected when using the pre-immune serum (**data not shown**). Finally, we performed western blot analysis to the recombinant AtPME2 purified by cation-exchange chromatography and showed the generic antiserum strongly detected the two AtPME2 protein bands separated at molecular mass ~35 kDa (**Figure 2D**). A strong antigen band is observed in the western blot with mass approaching 70 kDa, while no corresponding protein is observed in the stained protein gel (**Figure 2A**). We speculate this represents low amounts of either glycosylated unprocessed AtPME2 protein as observed in the hypocotyl and root blots (**Figure 2C**), or possibly dimers formed during electrophoresis.

To examine the role of the PRO-peptide for expressing active AtPME2 isoform in Pichia, we produced truncated forms by gradually deleting amino acids downstream from the putative signal peptide of the protein sequence (from 4 amino acids –"Δ4FL"- up to 212 amino acids –"Δ212FL"-, **Supplemental Figure 2A, 2B and 5**). Using the gel diffusion assay to follow PME activity, we showed that the first 20 amino-acids downstream the putative signal peptide are dispensable for the proper expression of active AtPME2 (**Supplemental Figure 5**). These results support the hypothesis that the PRO-domain directs folding of the full-length protein allowing interaction by a subtilisin-like Pichia protease with the processing sequence motifs in AtPME2, to provide subsequent secretion of an active isoform into the culture medium.

Biochemical characterization of AtPME2

The pH-dependency and sensitivity to inhibition by PMEI were determined for the purified AtPME2. Using the ruthenium red gel diffusion assay with a high DM pectins (> 85%) as a substrate, we showed the enzyme was the most active at neutral pH (7.5), although it was still active at pH 5 (**Figure 3A**). AtPME2 activity was inhibited at the three pHs tested (5, 6.3 and 7.5) by the previously reported pH-insensitive AtPMEI9 inhibitor protein (Hocq, Sénéchal, *et al.*, 2017). This inhibition was positively correlated with increasing quantities of AtPMEI9 (**Figure 3A**). In addition, AtPME2 could also be inhibited by pH-sensitive AtPMEI4 at pH 5 (**data not shown**).

We assessed AtPME2 activity on citrus pectins with varying esterification at the optimal pH 7.5. When using pectic substrates of low DA, AtPME2 activity was the strongest for DM 55 to 70% (40 nmol MeOH.min^{-1}. µg proteins^{-1}), and activity was reduced by ~half when using substrates of high (>85%) or low (24-30%) DM. AtPME2 was active on sugar beet pectins of DM 42% and DA 34%, suggesting acetylation of GalA residues may minimally affect the enzyme's activity (**Figure 3B**). Using the best substrate (pectins DM

55% - 70%) and the optimal pH of 7.5, we determined the kinetic parameters of the enzyme and showed that the Km was 0.481 mM and the Vmax was 0.019 nmol MeOH.min^{-1}.µg protein^{-1} (**Figure 3C**).

AtPME2 has a low degree of processivity in acidic conditions

In order to get precise insights into AtPME2 activity, we designed an experimental set-up to characterize its degree of processivity. We first digested the DM 55 to 70% with a fungal polygalacturonase (endo-PG from *Aspergillus aculeatus*) for 3 h to generate a population of HG oligogalacturonides (OGs) of various DP and DM. Following heat denaturation of PG activity, the processivity of AtPME2 was determined by characterizing the relative proportion of the resulting OGs, classified by DP and DM, after overnight incubation with 20 nmol AtPME2 at pH 8 and 80 nmol AtPME2 at pH 5 (to compensate for the lower PME activity at acidic pH). As a control, we used the commercially available PMEs extracted from Citrus peels, and which also present stronger activity at neutral pH compared to acidic pH (**data not shown**). The population of OG identified after PME digestion was then compared to that obtained in non PME-treated condition (named hereafter control pH 8 and control pH 5). In control samples, we were able to detect different methylated forms for each DP, with a peak of relative abundance corresponding on average to slightly more than 50% DM (*e.g.* GalA7Me4, GalA8Me4, GalA10Me6), in accordance with the mean DM of the pectins used as a substrate. At optimal pH 8, when considering oligos of DP comprised between 3 and 10, for instance DP 10 (GalA10), the different methylated forms detected in the control samples (GalA10Me5, GalA10Me6, GalA10Me7) were totally absent in AtPME2-treated OGs (**Figure 4A**). Similar results were obtained when using Citrus PME (**Supplemental Figure 6B)**.

When PME treatment (AtPME2 and CsPME) was performed at pH 5, results were strikingly different. For a given DP, the proportion of highly methylesterified forms (> 50% DM) decreased in the PME-treated samples compared to control pH 5 (**Figure 4B, Supplemental Figure 6B**). OGs with lower DM appeared when treatment with PME was performed (GalA10Me, GalA10Me2 and GalA10Me3, absent in control pH 5), and relative amount of higher DM decreased (GalA10Me5, GalA10Me6 and GalA10Me7) (**Figure 4B inset, Supplemental Figure 6B inset**). Results were similar for OGs of distinct DPs, including GalA6, GalA7, GalA8 and GalA9, with a shift in the abundance from highly methylesterified to low methylesterified forms of these OGs in PME-treated samples as compared to control pH5. It has to be mentioned that those differences in the DM

distributions are more pronounced when using AtPME2 compared to CsPME. For OGs of DP < 5, no differences were detected between samples, suggesting that PME2 and CsPME have a strong preference for substrates of DP > 5 at pH 5. Taken together, these results show that the degree of processivity of the two PMEs increases as the pH shifts from acidic towards neutral to alkaline pH.

The electrostatic potential of PMEs correlates with their processivity

Electrostatic properties have been identified as significant in order to rationalize the basis of PMEs processivity, with charge asymmetry along the binding groove being an important feature to promote the sliding of negatively charged, demethylesterified, polysaccharides (Mercadante *et al.*, 2014). We chose to compare the electrostatic potentials of the 2 PMEs whose modes of action were determined in this study, in addition to a fungal acidic PME from *Aspergillus niger*, AnPME, whose random mode of action at both pH has already been published (Duvetter *et al.*, 2006; Kent *et al.*, 2016; Cameron *et al.*, 2008). Interestingly, AtPME2 and CsPME4 (the major isoform present in the commercial PME from orange peel), which experimentally increase in processivity with increasing pH, show the largest differences in the electrostatic similarity indices, whereas AnPME, which has been indicated as a non-processive, acidic PME (Kent *et al.*, 2016) shows little differences across pH (**Figure 5A)**. Moreover, the projection of the electrostatic potential differences between acidic and alkaline pH on the protein surfaces, normalized to highlight the differences between AtPME2 and CsPME4 or AnPME, show a concentrated positive charge patterning in the binding groove, with the largest difference observed for CsPME4 and small to no difference (electrostatic potential difference close to 0) for AnPME; as expected from comparing the action of these PMEs experimentally **(Figure 5B)**.

Loss of function in AtPME2 mutants can alter pectin remodeling enzyme activities

To investigate AtPME2's role in controlling growth and development, two homozygous T-DNA insertional knockout (KO) lines, *pme2-1* (GK-835A09, in the third exon) and *pme2-2* (FLAG_445B05, in the first exon), were identified in Arabidopsis Col-0 and WS backgrounds respectively. RT-PCR analyses revealed that both mutant lines were KO at the transcript level (**Figure 6A**). Consistent with this, no tryptic peptides from the catalytic domain of AtPME2 were detected by proteomic analyses performed on cell wall-enriched protein fractions from *pme2-1* and *pme2-2* hypocotyls (**Supplemental Table IA**). This ultimately shows that *pme2* allelic mutants are KO at the protein level. This was further

supported by zymogram analysis where cell wall-enriched protein extracts from wild-type, *pme2-1* and *pme2-2* hypocotyls were resolved by isoelectric focusing (IEF) coupled with detection of PME activity. Results obtained showed no activity band at a pI of ~9 in the KO lines, which corresponds to the predicted pI of the mature part of AtPME2 (**Figure 6B**). No changes in the activity of the other PME isoforms were apparent, suggesting that the absence of the AtPME2 protein is likely to impact total PME activity. This was further confirmed by measuring pectin remodeling enzymes activities of cell wall-enriched proteins of 4 day-old dark-grown hypocotyls. As anticipated, we observed that the total PME activity decreased in *pme2* mutants compared to wild-type (**Figure 6C**). Total PG activity measured in the same type of extracts was also reduced by 10 % and 20 % in *pme2-1* and *pme2-2*, respectively (**Figure 6D**). In roots, total PME and PG activities were as well decreased in *pme2* mutants, albeit to a lesser extent compared to what was observed in dark-grown hypocotyls (**Supplemental Figure 7A and 7B**).

AtPME2 plays a role in controlling hypocotyl elongation through regulation of mechanical properties

To determine if changes in pectin remodeling enzyme activities may affect seedling development, we first assessed the effects of the mutations on primary root length and lateral root emergence. In our experimental conditions, elongation of primary root was slightly impaired in both mutants, although only significantly in Col-0 background, in relation to the decrease in the length of fully elongated cells (**Supplemental Figure 7C, data not shown)**. Considering AtPME2 expression pattern, lateral root density was also assessed and results showed significant lower density only for Col-0 allele (**Supplemental Figure 7D**).

We next followed etiolated hypocotyl elongation over a time-course. The rationale for etiolated hypocotyls includes: i) In the hypocotyl, cell length increased in an acropetal wave starting approximately 48 hours after sowing, ii) AtPME2 is highly expressed in the upper part of a 4 day-old growing hypocotyl, below the hook, where cells are strongly elongating, so that the absence of AtPME2 in mutants should alter their development. Thus, we hypothesized KO mutants lacking AtPME2 activity will show altered hypocotyl development. Kinematic analysis showed hypocotyl length was significantly different in both alleles, with a reduction of 10% as compared to wild-type (**Figure 7A**). The differences between wild-type and *pme2* mutants were more important from 72 h onwards, which corresponds to the rapid elongation phase. To assess if the decrease in the length is related to changes in the mechanical properties of the cell wall, we measured the stiffness (as apparent Young's

393 modulus) of the cell wall using atomic force microscopy (AFM) in the *pme2-1* mutant and its
394 corresponding wild-type Col-0. The stiffness of the epidermal cell wall at the basal part of 4-
395 day-old hypocotyls, was similar between *pme2* and WT Col-0 (**Figure 7B, bottom panel**). In
396 contrast, the apical part of hypocotyls (the zone where the promoter of *AtPME2* was shown to
397 be active) showed a 10% increase in cell wall stiffness in the *pme2-1* mutant, compared to
398 wild type (**Figure 7B, top panel**). As such, a more rigid cell wall in the *pme2-1* mutant could
399 restrict hypocotyl elongation. The Young's modulus measured at the top of dark-grown
400 hypocotyl was lower (~20 MPa) than that measured in the basal part (60 MPa), also reflecting
401 the difference of cell wall stiffness in relation to growth rate.
402
403

Discussion

How the mode of action by individual pectin methylesterases affect pectin's chemistry and the mechanical properties of plant cell walls remains unresolved. This is in part due to the difficulty for obtaining purified single isoforms from plant material and to co-expression of multiple isoforms from this very large gene family. Here, we report on AtPME2, a PME shown to be differentially expressed during lateral root emergence and dark-grown hypocotyl elongation. Starting from its production in heterologous system and full biochemical characterization, we describe how its mode of action varies as a function of ambient pH and assess the way this might control plant development.

While *AtPME2* gene was previously shown, among other *PMEs* and *PMEIs* (At3g49220, At3g14310, At4g25250…) to be highly expressed during the growth transition phase in dark-grown hypocotyls (Pelletier *et al.*, 2010) we show that the *AtPME2* promoter is highly active at the top of hypocotyls in 3 to 4 day-old dark grown seedlings (**Figure 1**). At 4 days, mainly the cells below the hook undergo elongation (Refrégier *et al.*, 2004; Daher *et al.*, 2018; Peaucelle *et al.*, 2015). The *AtPME2* promoter is also highly active in the root elongation zone, probably in relation with cell elongation, and during lateral root formation, as suggested by previous data sets (Brady *et al.*, 2007; Hruz *et al.*, 2008) and recently confirmed using RNA sequencing and immunocytochemistry (Wachsman *et al.*, 2020). In lateral root primordia, the promoter's activity initiates at stage VI before emergence (Malamy and Benfey, 1997), suggesting a role with other pectin remodeling enzymes (including PG) in the process of lateral rhizogenesis (Swarup *et al.*, 2008; Kumpf *et al.*, 2013; Hocq *et al.*, 2020). Our results are in accordance with this hypothesis (**Supplemental Figure 7**), which was recently confirmed by a study showing AtPME2 to be of prime importance for determining lateral root emergence through the control by the root clock (Wachsman *et al.*, 2020). The authors showed that the *pme2* mutant had indeed reduced lateral root density compared to wild-type.

Peptide mass fingerprinting analyses identified AtPME2 and other PME isoforms present in the cell wall-associated proteome from dark-grown hypocotyls and radicles in seedling (**Supplemental table IA, B**). Their presence as mature, processed proteins supports SBT-mediated processing occurs in the cell before their deposition at the apoplast. Using C-terminal translational fusion, we showed AtPME2 present both at the cell wall and in the cytoplasm, further suggesting that its maturation occurs during transport (**Figure 1A**). The differential detection of peptides mapping only the mature PMEs (i.e., the catalytic domain) shown for other plant PME (in similar or distinct organs) indicates a ubiquitous processing

mechanism (San Clemente and Jamet, 2015; Sénéchal *et al.*, 2015; Hervé *et al.*, 2016; Nguyen-Kim *et al.*, 2016).

Obtaining sufficient amounts of plant PME for biochemical analysis, through their expression in a non-host system, has often turned out to be challenging, despite early reports showing that AtPME31 and AtPME12 can be expressed in *E. Coli* (Dedeurwaerder *et al.*, 2009; Cheong *et al.*, 2019), or that an acidic PME from Jelly fig can be produced in yeast (Peng *et al.*, 2005). While our initial attempt to produce AtPME2 (group 2 plant PME) directly as a mature form in *Pichia* proved unfeasible, we subsequently showed the PRO domain was required for proper cleavage and release of a functional PME. Thus, catalytically active AtPME2 was achieved by expressing the full-length protein minus the plant signal peptide (**Figure 3; Supplemental Figure 5**). We further determined using successive N-terminus deletions of the protein sequence, that the expression of an active AtPME2 in *Pichia pastoris* requires a large part (~200 amino acids) of the N-terminal extension (**Supplemental Figure 2 and 5**). Our results support the hypothesis that the PRO part supports recognition processing motifs RKLK and RRLL in AtPME2 by endogenous yeast subtilisins, including KEX2 and SUB2 (Bader *et al.*, 2008; Salamin *et al.*, 2010). *In planta*, PME and SBTs are co-expressed during development and the S1P-mediated processing of group 2 PMEs is required for the export of active enzymes in the cell wall (Wolf *et al.*, 2009). It was further suggested that the PRO-region inhibits group 2 PMEs activity during transport through the secretory pathway (Bosch, 2005; Bosch and Hepler, 2005; Dorokhov *et al.*, 2006). We now have the tools to decipher the sequence and structural determinants of AtPME2 processing: Using Pichia, site-directed mutagenesis of the processing motifs, as well as the generic anti-PME antibody characterized within the course of this study, we could assess the *in vitro* interaction between AtPME2 (or any PME) with purified SBT. In addition, through co-immunoprecipitation analyses, the anti-PME antibody will be a unique tool to help identifying PME-SBT, as well as PME-PMEI complexes present in the apoplast *in vivo*.

Recombinant expression of functional AtPME2 enabled its biochemical characterization, showing a weakly alkaline pH activity optimum (**Figure 3A**), like Arabidopsis AtPME3 and AtPME31 (Dedeurwaerder *et al.*, 2009; Sénéchal *et al.*, 2015). The predicted pI~9 for AtPME2 might explain the pH-dependency of the enzyme's activity as it was previously shown that most plant and bacterial PMEs have a neutral to alkaline pI, while fungal enzymes are acidic (Sénéchal, Wattier, *et al.*, 2014). AtPME2 is inhibited *in vitro* by both pH-sensitive and pH-insensitive PMEIs (AtPMEI4 (data not shown) and AtPMEI9 (**Figure 3A**), respectively) (Hocq, Sénéchal, *et al.*, 2017). This suggests that it might be the

target of multiple inhibitors at the cell wall, which further questions the role of such diversity of PME-PMEI interactions.

We applied a newly developed LC-MS/MS oligosaccharide-profiling approach, that determines DP and methylation of OGs, for analysing PME processivity (Hocq *et al.*, 2020; Voxeur *et al.*, 2019). We determined that AtPME2 presents a non-processive mode of action at pH 5, which is approximate to the apoplastic cell wall pH , while at its activity optimum pH 8, it showed a processive mode of action (Hocq *et al.*, 2017). This was demonstrated in **Figure 4A** where with PME treatment at alkaline pH the unmethylated OG trimer and tetramer were the predominant end-products accumulated. These OGs can result from the residual activity of Aspergillus PG in the reaction mixture: in absence of calcium *in vitro*, long blocks of unmethylated HG created by processive demethylesterification of pectins at pH8 are preferential substrates, leading to hydrolysis of the OGs pool. In contrast, AtPME2 random demethylesterification occuring at pH 5 resulted in intermediate DP OGs, of decreased mean DM, which show less affinity for Aspergillus PG (**Figure 4B**).

Processive behaviour by plant and bacterial PMEs have been described in detail (Willats *et al.*, 2006; Jolie *et al.*, 2010), and the structural determinants of the processivity of the *Erwinia* PME was unraveled using molecular dynamic (MD) simulations (Mercadante *et al.*, 2014; Mercadante *et al.*, 2013), where the rotation of monosaccharide subunits in the binding groove of the enzyme was shown to be a key determinant of the processivity. In contrast to plant and bacterial PMEs, fungal enzymes are often regarded as being non processive. The recent elucidation of the 3D structure of a non-processive, salt-requiring, PME from *Aspergillus niger* demonstrated key differences between processive and non-processive isoforms, highlighting the importance of the electrostatic potentials of the enzymes in determining their processivity (Kent *et al.*, 2016). This is in accordance with our experimental observations of the differences in processivity observed at different pH for the plant PMEs. Differences in the electrostatic similarity indices (Blomberg *et al.*, 1999; Wade *et al.*, 2001) calculated at two different pH can therefore yield an understanding of the different properties of PMEs at different pH. The comparison of the electrostatic potentials of PMEs either active in basic or acidic conditions, interestingly suggests that differences between the electrostatic potentials at acidic and alkaline pH are particularly concentrated in proximity of subsites -2 and -3, which have been identified as preferentially docking negatively charged de-methylesterified galacturonic acid monomers; with non-processive AnPME showing the absence of positive patches in these subsites. Our results clearly demonstrate that the pH-dependency of the mode of action of PMEs, previously suggested in early reports on apple

PME (Catoire *et al.*, 1998), might be a key to fine-tune enzymes activity in cell wall microenvironments defined by local pH. Localized changes in apoplastic pH were indeed previously shown to be of major importance for auxin-mediated hypocotyl elongation (Fendrych *et al.*, 2016). As such, pH-dependent changes in PME mode of action might explain a number of unexpected results linking pectin chemistry to cell wall mechanical properties gathered over the last 10 years. Based on *in vitro* studies on pectin-based gels, it was assumed that demethylesterification of pectins by plant PME should lead to large stretches of negatively-charged GalA that can cross-link with calcium ions, stiffening the wall (Willats *et al.*, 2001). However, this scheme appears contradictory with reports showing that overexpressing plant PMEs lead to reduced stiffness of the wall, through decreased values of the Young's modulus (Peaucelle, Braybrook, *et al.*, 2011; Peaucelle *et al.*, 2015; Wang *et al.*, 2020). Supported by our results on AtPME2, a possible explanation of these apparent contradictory reports might reside in the fact that, within the acidic context of the cell wall, PME mode of action is not what was inferred from *in vitro* studies and may change according to pH microenvironments.

To assess whether the absence of AtPME2 can have consequences on development, we analyzed two T-DNA alleles, *pme2-1* and *pme2-2*, knock-out at the gene and protein levels. We showed that *pme2* mutants had reduced root length as well as reduced lateral roots density, compared to the control. Our data further demonstrated that dark-grown hypocotyls of *pme2* mutants were shorter compared to wild-type, which correlated with an increase in cell wall's Young's Modulus in elongating cells of this organ, at the top of the hypocotyl. In addition, these mutants showed decreased PME as well as reduced PG activities. It therefore appears that, in *pme2* mutants, higher methylesterification of pectins would prevent their hydrolysis by PGs, reducing elongation through stiffening the walls. Our results are in accordance with those presented by Peaucelle et al. (Peaucelle *et al.*, 2011; Peaucelle *et al.*, 2015), either in elongating organs such as our model, or in meristems, where softening of the wall is a prerequisite for organ initiation. In both cases, softening of the wall was correlated with higher 2F4 labelling (Peaucelle *et al.*, 2015; Braybrook and Peaucelle, 2013). According to our results, in the acidic context of the cell wall, AtPME2 would participate to pectin demethylesterification by randomly acting on the HG chains, leading to the creation of substrates for PG, and consequent destructuration of HG. The somehow contrasting reports linking pectins to cell wall mechanics (Daher *et al.*, 2018; Peaucelle *et al.*, 2015) might be partially explained by our results, suggesting that pH plays a key role in changing PME processivity, thereby affecting pectin mechanical properties. Our biochemical data support a

model for which the regulation of PME activity by microdomains of distinct pH might be a key to link pectin chemistry to cell wall mechanics.

Material and Methods

Plant material and growth conditions

Two *Arabidopsis thaliana* T-DNA insertion lines in the Columbia-0 (Col-0) and WS (Wassilewskija) ecotypes were used for *At1g53830* (*PME2*): *pme2-1* (GK-835A09, in the third exon) and *pme2-2* (FLAG445B05, in the first exon). Homozygous lines were isolated using gene-specific primers, *pme2-1* (F 5'- GACGGAAGCGGTGACTTTAC-3' and R 5'-AGTGTCCAACGCAAAACTCC-3'); *pme2-2* (F 5'-CTCAACACTATACCCGGA-3' and R 5'-ACTTTCCTATCGGCGTCG-3') as well as T-DNA specific primers for GK (F 5'-ATATTGACCATCATACTCATTGC-3') and FLAG (F 5'-CTACAAATTGCCTTTTCTTATCGAC-3'). For RT-qPCR analysis of *AtPME2* gene expression, seeds from Columbia-0 (Col-0) background were sowed either on soil or on plates containing ½ MS solid media and placed two days in cold chamber for stratification. Seeds in soil were then transferred in greenhouse, and plates in growth chambers, in the following conditions: 16h photoperiod at 120 µmol m^{-2} s^{-1} and at 23°C). For dark-grown hypocotyls, seeds were sterilized and sown *in vitro* as previously described (Hocq *et al.*, 2020). Plates were incubated at 4°C for 2 days for stratification and transferred to the light (120µmoles/m²/s) for 6 hours to induce germination. Plates were placed in the dark, wrapped with three layers of aluminum foil and incubated in the same conditions of temperature. Organs were collected, frozen in liquid nitrogen and stored at -80°C before use. For kinetic phenotyping of hypocotyls, seeds from the four genotypes were sterilized and sown *in vitro* as above mentioned previously described (Hocq *et al.*, 2020). They were then put in the dark at 21°C for 6 days in a phenobox chamber. This specific growth chamber is designed to receive 27 square Petri dishes (12mm*12mm) and to allow automatic image acquisition of each one using a 36 Mpix D810 camera (Nikon, Champigny sur Marne, France) fixed onto a robotic arm (Optimalog, Saint-Cyr-sur-Loire, France). Pictures were taken every 4 hours, during the first 20 hours, and then every 2 hours. Images from each seedling were analyzed by a specific software (Optimalog) for measurement of hypocotyl length. For each biological replicate, at least 40 hypocotyls were analyzed.

Analysis of gene expression by RT-qPCR

Total RNAs extraction, cDNA synthesis and RT-qPCR experiments were performed as previously described (Hocq *et al.*, 2020) using specific primers for *AtPME2* (F 5'-TACGACGACGCCGATAGGAAAG-3' and R 5'-ATGTGCTCCACGTGTACCTGAC-3'). Relative expression was normalized according to the most stable reference genes, identified with Genorm in each sample panels (Vandesompele et al., 2002): *CLA* when the expression of *AtPME2* was measured in the different organs (*At5g46630*, CLA-F 5'–GTTTGGGAGAAGAGCGGTTA-3' and CLA-R 5'-CTGATGTCACTGAACCTGAACTG-3') and *TIP41* during the time course of dark-grown hypocotyl development (At4G34270, TIP41-F 5'-GCTCATCGGTACGCTCTTTT-3' and TIP41R 5'-TCCATCAGTCAGAGGCTTCC-3'). Method used to determine relative expression was previously described in Sénéchal *et al.*(Sénéchal *et al.*, 2014). Two to three biological replicates were realized, with two technical replicates each.

Promoter amplification, plant transformation and GUS staining

Amplification of the promoter sequence of At*PME2* (~2 kb upstream of the *AtPME2* transcription start) was performed using the specific primers F 5'-**AAGCT**TGTACAATGATGGTTCTATTGT-3' and R 5'-**TCTAGA**GGTGGAATAGGGTTTATATTG-3', with AAGCTT and TCTAGA being recognition sites for *Hind*III and *Xba*I enzymes respectively. The purified PCR product was subsequently cloned into pBI101.3 (Ozyme, Saint-Cyr l'Ecole, France), upstream of GUS coding gene. Transformation, plant selection, GUS staining and image acquisition was as previously described (Hocq *et al.*, 2020).

Fusion of *AtPME2* coding sequence with fluorescent tag and confocal imaging

At1g53830 coding sequence was amplified from Riken pda01692 by PCR using Phusion Hot Start II DNA Polymerase (Thermo Scientific, F549) with two specific primers: F 5'- **CACC**ATGGCACCAATCAAAG -3' and R-5'-AAGACTTAACGAGAAAGGAA-3'. Coding sequence was inserted in a first vector, pENTR™ Directional TOPO® (Invitrogen), then transferred in binary vector pGBW454 *via* LR reaction (Gateway LR Reaction Kit, Invitrogen) resulting in the translational fusion of *At*PME2 with GFP (green fluorescent protein) sequences under the control of CaMV-P35S promotor. *Rhizobium radiobacter* (C58C1) was transformed with pGBW405 recombinant vector *via* electroporation and used for transformation of Arabidopsis. After selection of transformants, roots were incubated with propodium iodine (IP, 0.1 mg ml^{-1}, Sigma-Aldrich, # P4864, St. Louis, MO, USA) for 20

minutes, then transferred in 1 M sorbitol solution to plasmolyze cells before observation under confocal microscope (Zeiss, LMS 780). Excitation wavelengths are 370-560 nm and 488 nm for IP and GFP respectively, and emission wavelengths are 631 nm and 493-549 nm in the same order.

AtPME2 cloning and overexpression in *Pichia pastoris* and purification

The coding sequence, minus the signal peptide, of *At1g53830* was amplified from Riken pda01692, using the Phusion Hot Start II DNA Polymerase and specific primers (F 5'-**CTGCAG**GAGCCACAACAACAAAC -3' and R 5'-**GCGGCCG**CAAGACTTAACGAGAAAGGA -3'). The amplified full-length sequence, referred as "FL", was cloned in frame with polyHis sequence into pPICZαB (ThermoFisher Invitrogen™) after restriction by *PstI-NotI*, as previously described (Hocq *et al*. 2020). For truncation of the N-terminus PRO part of AtPME2, sequences were amplified using the primers described in **Supplemental Figure 2** and cloned in the same conditions. These sequences were referred as Δ4FL, Δ8FL, Δ16FL, Δ20FL, Δ40Fl, Δ115FL, Δ192FL and Δ212FL. After *E. coli* TOP10 (Invitrogen) transformation, recombinant plasmid was verified by sequencing, and the linearized construct was inserted into X-33 *Pichia pastoris* for protein expression. Selection of transformants and cultures were performed as previously described (Hocq *et al.*, 2020). Culture supernatants were recovered following centrifugation, then applied onto a CM-FF Hi trap cation-exchange column following the manufacturer's instructions (GE-Healthcare). Fractions with PME activity were pooled and concentrated using 10kDa Amicon filtration column before desalting using a PD spin trap G-25 column (GE-Healthcare). For LC-MS determination of the mode of action, aliquots of AtPME2 were exchanged into 100 mM ammonium acetate pH 5, or 20 mM Tris HCl pH 8 using Amicon® Ultra 0.5 mL Centrifugal Filters (Millipore) following manufacturer's recommendations.

Mass spectrometry analysis of PMEs

Cell wall-enriched protein fractions from 4 day-old dark-grown hypocotyls (WT and *pme2* mutants) and roots (WT) were extracted from 50 mg frozen fine powder according to method previously described (Sénéchal, Graff, *et al.*, 2014). Equal amounts of proteins were resolved on SDS-PAGE for each condition. Tryptic peptides from excised bands were separated and analysed as previously described (Sénéchal, Graff, *et al.*, 2014). Following purification of AtPME2 by cation exchange chromatography, bands corresponding to putative mature and PRO part were excised and treated as described above.

642

643 **PME-specific antibodies and Western blot analysis**

644 For Western blot analysis of recombinant AtPME2, AtPME3 (Sénéchal *et al.*, 2015),
645 purified native sweet orange and tomato PMEs (Savary *et al.*, 2010; Savary *et al.*, 2013;
646 Savary, 2001), and cell wall-enriched protein extracts from dark-grown hypocotyls and roots,
647 were separated onto a SDS-PAGE and supernatant proteins was transferred from resolving gel
648 to Hybond-P PVDF transfer membrane (GE Healthcare, Amersham™ RPN303F) using the
649 manufacturer's instructions and a Trans-Blot TURBO Transfer System (Bio-Rad, 170-4155)
650 at 0.1A for 30 min. Blotted membranes were blocked with BSA and incubated for 2 h at room
651 temperature with 1:3000 dilution of anti-PME primary antibody. This polyclonal antibody
652 was raised in rabbits against a synthetic peptide (CKTYLGRPWKEYSRT) (Genscript,
653 Piscataway, NJ) that includes the highly conserved amino acid sequence including residue in
654 the catalytic site of PMEs (Markovič and Janeček, 2004) and was shown to cross-react with
655 plant PMEs, including *Citrus sinensis* and tomato fruit PMEs, representing multiple gene
656 isoforms. Blotted membrane was probed with 1:5000 dilution of anti-rabbit secondary
657 antibody coupled with peroxidase (ThermoFisher, 31460), followed by detection with the
658 chemiluminescent substrate (ECL™ Prime Western Blotting System, GE Healthcare,
659 RPN2232).

660

661 **Enzymatic activity assays**

662 Total PME activity was quantified on cell wall-enriched protein extracts using
663 commercial citrus pectins (DM >85% P9561, Sigma-Aldrich) and the alcohol oxidase-
664 coupled colorimetric assay (Klavons and Bennet, 1986; L'Enfant et al., 2015). Substrate
665 specificity of recombinant AtPME2 activity was determined at pH 7.5 and 28°C using
666 commercial citrus pectin (Sigma-Aldrich, DM >85%, P9561; DM 55-70, P9436; DM 20-
667 34%, P9311), sugar beet pectin (DM 42%, degree of acetylation 31% (CPKelco). Results
668 were expressed as nmol MeOH min^{-1} μg^{-1} of protein using a methanol standard curve. The
669 kinetic parameters, V_{max} and K_m, were determined on citrus pectin (DM 55-70%, Sigma-
670 Aldrich, P9436). The reactions were performed with 3 to 6 replicates using substrate
671 concentrations ranging from 0.125 to 2 mg mL^{-1}. The kinetic data were calculated by the
672 Hanes-Wolf plot. Total PG activity from cell wall enriched dark-grown hypocotyl extract was
673 determined as previously described (Hocq *et al.*, 2020).

674

675 **Gel diffusion assays**

The effects of pH on purified AtPME2 activity and inhibition assays were quantified by gel diffusion (Downie *et al.*, 1998) with some modifications (Ren and Kermode, 2000). For each inhibition experiments, 5 µg of purified protein were pre-incubated for 30 min at room temperature with AtPMEI9 in a final volume of 12 µL as described previously (Hocq *et al.*, 2017). The PME activity in supernatants from various deletion mutants was assayed in the same conditions. The reaction mixtures were loaded into each well in the gels containing 0.1 % citrus pectin (DM >85 %, Sigma-Aldrich, P9561) and prepared at pH 5, pH 6.3, and pH 7.6. After incubation at 37 °C for 16 h, gels were stained with a 0.02 % (w/v) ruthenium red solution for 1 h and washed with distilled water. Diameters of the red halos, correspond to demethylesterified/acidic pectins, and reflect PME activity.

Oligosaccharide mass oligoprofiling

To determine the mode of action of recombinant AtPME2, first, 0.4% (w:v) citrus pectin DM 55-70 % (Sigma, Cat. No. P9436) were first subjected to a 2 h digestion in ammonium acetate buffer 100mM pH4 at 40 °C by 2.9 $U.mL^{-1}$ of *Aspergillus acuelatus endo*-polygalacturonase M2 (Megazyme, Bray, Ireland) to generate OGs which differ in their degrees of polymerization and methylesterification. After addition of 1 volume absolute ethanol and centrifugation (5 min, 5000g), the upper phase containing OGs was divided in two tubes, evaporated using speed vac, and re-suspending either in ammonium acetate 100mM pH 5, or in Tris HCl 20mM pH 8. After heat-inactivation of PG, OGs were treated for 16h at 40°C by 80 nmol/min of purified AtPME2 either at pH 5 (Buffer) or 20 nmol/min at pH 8 (Buffer) in order to compensate for the difference in activity measured at both pH. Chromatographic separation of OGs by size exclusion chromatography (SEC), MS-detection and data acquisition and processing were performed as previously described (Hocq *et al.*, 2020).

Calculation and comparison of protein electrostatics

For structural homology modeling of AtPME2 and CsPME4 protein structure, we used I-TASSER prediction software (https://zhanglab.ccmb.med.umich.edu/I-TASSER/). 3D models of putative mature parts of Arabidopsis AtPME2 and Orange PME were created using *D. carota* PME (P83218, PDB:1GQ8, (Johansson *et al.*, 2002)) as a starting model. The calculation of the electrostatic potential was obtained by solving the linearized version of the Poisson-Boltzmann equation. Atomic radii and partial charges were assigned to each atom according to the AMBER99 force field parameters (Wang *et al.*, 2000), using the PDB2PQR

software version 2.1.1 (Dolinsky *et al.*, 2004). The structures of AtPME2, AnPME and CsPME4 were superimposed and electrostatic potentials were calculated using APBS version 3 (Baker *et al.*, 2001), considering the protonation states empirically estimated using the PROPKA software, version 3.3 (Søndergaard *et al.*, 2011) at either pH 5.0 or pH 8.0. The solution of the Poisson-Boltzmann equation was discretized on a grid of dimensions 19.3 nm^3 and grid spacing of 0.6 Å. The grid was centered on the C_α atom of one of the PMEs catalytic aspartic acid residues, conserved across PMEs. In particular, Asp157, Asp189 and Asp153 were chosen to center the grids of AtPME2, AnPME and CsPME4 respectively. Solvent dielectric was set at a value of 78.5 to account for an aqueous environment, whereas solute dielectric was set to 4.0 and temperature set at 298.15 K. Potentials calculated at alkaline pH were then subtracted, grid point by grid point, from the potentials calculated at acidic pH, to obtain an electrostatic potential difference. A numerical comparison of the electrostatic potentials was achieved by calculating electrostatic similarity indices (Blomberg *et al.*, 1999; Wade *et al.*, 2001). We calculated the cross-product between two electrostatic potentials calculated at each grid point as follows:

$$SI^{H}_{a,b} = \frac{2\phi_a(i,j,k)\phi_b(i,j,k)}{\left(\phi_a^2(i,j,k) + \phi_b^2(i,j,k)\right)}$$

Where $\phi_a^2(i,j,k)$ and $\phi_b^2(i,j,k)$ are the electrostatic potentials calculated at the grid points *i,j,k* for proteins *a* and *b* (Blomberg *et al.*, 1999; Wade *et al.*, 2001). In order to compare the differences in electrostatic potentials in acidic and basic environments, electrostatic similarity indices were calculated between the electrostatic potentials of the same PME obtained at pH 5.0 and pH 8.0.

Atomic Force Microscopy (AFM) measurements

The protocol was adapted from (Milani *et al.*, 2011) and applied to wild type and *pme2-1* hypocotyls at 3 days after induction of germination. Hypocotyls were removed from the foiled boxes and then immobilized in 6 cm-diameter Petri dishes by gluing them with a biocompatible glue (Reprorubber-Thin Pour, Flexbar Ref. 16135) and covered with sterilized Milli-Q purified water to maintain hydration during all experiments. All mechanical measurements were performed as close as possible (typically ~ 1 mm) to the hook (**Supplemental Figure 8A**) or to the collet and the duration of measurements ranged 45-60 min for each sample. We used a JPK Nanowizard III atomic force microscope, operated with

the JPK Nanowizard software 6.0.41. In order to characterize cell wall properties locally, we used two types of cantilever with pyramidal tip and spring constants 5N/m (TAP150/MPP-12100-10, Bruker) and 6N/m (RTESP-150, Bruker), aiming at probing the wall down to depths ~100nm. Cantilevers were calibrated following the standard thermal noise method. Deflection sensitivity was measured by indenting on sapphire in Milli-Q water. Spring constant was deduced from the first normal mode peak of its thermal noise spectrum, based on a single harmonic oscillator model. The same cantilever was used for several experiments in different days, as long as possible. Cantilevers were systematically cleaned, except when new. Before experiments, cantilevers were immerged 10 min in 2% Hellmanex III (Merck), 10 min in Milli-Q water, and then 5 min in 70% ethanol. Following experiments, cantilevers were rinsed in Milli-Q water and then in 70% ethanol. We analysed three regions of size 60µmx60µm, spanning two or three cells from the top (farthest from the dish) of each hypocotyl. We first acquired a topographic image (**Supplemental Figure 8B**) using the Quantitative Imaging mode (QI), with a pixel size of 2µm x 2µm and a force set point of 10nN; the sample rate of cantilever deflection was 5 kHz for approach and 25 kHz for retract. We determined manually about 60 points along the top of visible cells (**Supplemental Figure 8B**) to avoid any biases due to slope of the sample surface. We then switched to force spectroscopy mode to obtain force-depth curves at these points. We used a trigger force of 400 nN (Z closed loop on) chosen to reach a maximum indentation depth in the range 100 to 400 nm, a ramp size (Z length) of 1.5 µm, approach and retract velocities of 10 µm/s, and a sample rate of 10 kHz. We analysed curves using JPK Data Processing software (versions 6.1.79 to 6.1.157). Curves were flattened by removing a linear fit to the baseline (non-contact part). The contact point was first estimated using the first change in sign of force starting from the maximal force.

Indentation depth curve was calculated as height minus tip deflection. Apparent Young's modulus was obtained by fitting the 0-100 µm depth range of the force-depth curve with the Sneddon model for a cone of half-angle 18°, assuming a Poisson ratio of 0.3 for the cell wall (**Supplemental Figure 8C)**. All measurements for a given hypocotyl were pooled together and we computed the corresponding average modulus.

Statistical analysis

Data represent the mean ± SE and were treated with R software (R development Core Team, 2008). Normality of data and equality of variances were assessed using Shapiro-Wilk and F-

775 tests, respectively. Non-parametric Wilcoxon test was carried out for pairwise comparisons.
776 Significant differences between two groups were determined as highly significant for $p <$
777 0.001 (***), significant for $p < 0.1$ (**), and moderately significant for $p < 0.05$ (*), while ns
778 indicates non-significant differences.
779

Acknowledgements

This work was supported by grants from the Agence Nationale de la Recherche (ANR-12-BSV5-0001 GALAPAGOS and ANR PECTOSIGN). LH was recipient of a studentship from the "Trans Channel Wallnet" project, which was selected by the INTERREG IVA program France (Channel) – England European cross-border cooperation program. The financial support from the Institut Universitaire de France (IUF) to JP is gratefully acknowledged.

Author's contribution

L.H., O.H., A.V., F.F., CP-R, J.S., F.S., S.B., S.P., V.B., P.M., M-F.N., D.M. performed research and analyzed the results. D.M., B.J.S., T.B., A.B., VL and JP designed the research. V.L. and J.P. managed the project. V.L., J.P. wrote the manuscript with input from D.M., B.J.S. and A.B.

Conflicts of interest

There are no conflicts of interest.

Bibliography

Andres-Robin, A., Reymond, M.C., Dupire, A., et al. (2018) Evidence for the regulation of gynoecium morphogenesis by ETTIN via cell wall dynamics. *Plant Physiol.*, 178, 1222–1232.

Bader, O., Krauke, Y. and Hube, B. (2008) Processing of predicted substrates of fungal Kex2 proteinases from Candida albicans, C. glabrata, Saccharomyces cerevisiae and Pichia pastoris. *BMC Microbiol.*, 8, 116. Available at: http://bmcmicrobiol.biomedcentral.com/articles/10.1186/1471-2180-8-116 [Accessed June 11, 2020].

Baker, N.A., Sept, D., Joseph, S., Holst, M.J. and McCammon, J.A. (2001) Electrostatics of nanosystems: Application to microtubules and the ribosome. *Proc. Natl. Acad. Sci. U. S. A.*, 98, 10037–10041. Available at: https://pubmed.ncbi.nlm.nih.gov/11517324/ [Accessed November 24, 2020].

Blomberg, N., Gabdoulline, R.R., Nilges, M. and Wade, R.C. (1999) Classification of protein sequences by homology modeling and quantitative analysis of electrostatic similarity.

Proteins Struct. Funct. Genet., 37, 379–387. Available at: https://onlinelibrary.wiley.com/doi/full/10.1002/%28SICI%291097-0134%2819991115%2937%3A3%3C379%3A%3AAID-PROT6%3E3.0.CO%3B2-K [Accessed November 17, 2020].

Bosch, M. (2005) Pectin Methylesterases and Pectin Dynamics in Pollen Tubes. *Plant Cell Online*, 17, 3219–3226. Available at: http://www.plantcell.org/cgi/doi/10.1105/tpc.105.037473.

Bosch, M. and Hepler, P.K. (2005) Pectin methylesterases and pectin dynamics in pollen tubes. *Plant Cell*, 17, 3219–3226.

Brady, S.M., Orlando, D.A., Lee, J.Y., Wang, J.Y., Koch, J., Dinneny, J.R., Mace, D., Ohler, U. and Benfey, P.N. (2007) A high-resolution root spatiotemporal map reveals dominant expression patterns. *Science (80-.).*, 318, 801–806.

Braybrook, S.A. and Peaucelle, A. (2013) Mechano-chemical aspects of organ formation in Arabidopsis thaliana: the relationship between auxin and pectin. *PLoS One*, 8, e57813–e57813. Available at: https://pubmed.ncbi.nlm.nih.gov/23554870.

Cameron, R.G., Luzio, G.A., Goodner, K. and Williams, M.A.K. (2008) Demethylation of a model homogalacturonan with a salt-independent pectin methylesterase from citrus: I. Effect of pH on demethylated block size, block number and enzyme mode of action. *Carbohydr. Polym.*, 71, 287–299. Available at: http://www.sciencedirect.com/science/article/pii/S0144861707003530.

Catoire, L., Pierron, M., Morvan, C., Hervé Du Penhoat, C. and Goldberg, R.E. (1998) *Investigation of the Action Patterns of Pectinmethylesterase Isoforms through Kinetic Analyses and NMR Spectroscopy IMPLICATIONS IN CELL WALL EXPANSION**, Available at: http://www.jbc.org/ [Accessed January 6, 2020].

Cheong, M.S., Lee, D.Y., Seo, K.H., Choi, G.H., Song, Y.H., Park, K.H. and Kim, J.H. (2019) Phenylephrine, a small molecule, inhibits pectin methylesterases. *Biochem. Biophys. Res. Commun.*, 508, 320–325.

Daher, F.B., Chen, Y., Bozorg, B., Clough, J., Jönsson, H. and Braybrook, S.A. (2018) Anisotropic growth is achieved through the additive mechanical effect of material anisotropy and elastic asymmetry. *Elife*, 7. Available at: https://elifesciences.org/articles/38161 [Accessed February 4, 2019].

Dedeurwaerder, S., Menu-Bouaouiche, L., Mareck, A., Lerouge, P. and Guerineau, F. (2009) Activity of an atypical Arabidopsis thaliana pectin methylesterase. *Planta*, 229, 311–321.

Denès, J.M., Baron, A., Renard, C.M.G.C., Péan, C. and Drilleau, J.F. (2000) Different action

patterns for apple pectin methylesterase at pH 7.0 and 4.5. *Carbohydr. Res.*, 327, 385–93. Available at: http://www.ncbi.nlm.nih.gov/pubmed/10990023 [Accessed January 6, 2020].

Dixit, S., Upadhyay, S.K., Singh, H., Pandey, B., Chandrashekar, K. and Verma, P.C. (2013) Pectin methylesterase of Datura species, purification, and characterization from Datura stramonium and its application. *Plant Signal. Behav.*, 8.

Dolinsky, T.J., Nielsen, J.E., McCammon, J.A. and Baker, N.A. (2004) PDB2PQR: An automated pipeline for the setup of Poisson-Boltzmann electrostatics calculations. *Nucleic Acids Res.*, 32. Available at: https://pubmed.ncbi.nlm.nih.gov/15215472/ [Accessed November 24, 2020].

Dorokhov, Y.L., Skurat, E. V., Frolova, O.Y., et al. (2006) Role of the leader sequence in tobacco pectin methylesterase secretion. *FEBS Lett.*, 580, 3329–3334. Available at: http://doi.wiley.com/10.1016/j.febslet.2006.04.090 [Accessed June 11, 2020].

Downie, B., Dirk, L.M.A., Hadfield, K.A., Wilkins, T.A., Bennett, A.B. and Bradford, K.J. (1998) A gel diffusion assay for quantification of pectin methylesterase activity. *Anal. Biochem.*, 264, 149–157.

Duvetter, T., Fraeye, I., Sila, D.N., Verlent, I., Smout, C., Hendrickx, M. and Loey, A. Van (2006) Mode of De-esterification of Alkaline and Acidic Pectin Methyl Esterases at Different pH Conditions. *J. Agric. Food Chem.*, 54, 7825–7831. Available at: https://doi.org/10.1021/jf060013h.

Fendrych, M., Leung, J. and Friml, J. (2016) TIR1/AFB-Aux/IAA auxin perception mediates rapid cell wall acidification and growth of Arabidopsis hypocotyls. *Elife*, 5, e19048. Available at: https://pubmed.ncbi.nlm.nih.gov/27627746.

Francoz, E., Ranocha, P., Ru, A. Le, Martinez, Y., Fourquaux, I., Jauneau, A., Dunand, C. and Burlat, V. (2019) Pectin Demethylesterification Generates Platforms that Anchor Peroxidases to Remodel Plant Cell Wall Domains. *Dev. Cell*, 48, 261-276.e8.

Fries, M., Ihrig, J., Brocklehurst, K., Shevchik, V.E. and Pickersgill, R.W. (2007) Molecular basis of the activity of the phytopathogen pectin methylesterase. *EMBO J.*, 26, 3879–3887. Available at: http://emboj.embopress.org/cgi/doi/10.1038/sj.emboj.7601816 [Accessed June 5, 2020].

Goldberg, R., Morvan, C., Jauneau, A. and Jarvis, M.C. (1996) Methyl-esterification, de-esterification and gelation of pectins in the primary cell wall. *Prog. Biotechnol.*, 14, 151–172.

Hervé, V., Duruflé, H., San Clemente, H., Albenne, C., Balliau, T., Zivy, M., Dunand, C. and

879 Jamet, E. (2016) An enlarged cell wall proteome of *Arabidopsis thaliana* rosettes.
880 *Proteomics*, 16, 3183–3187. Available at: http://doi.wiley.com/10.1002/pmic.201600290
881 [Accessed June 11, 2020].
882 Hewezi, T., Howe, P., Maier, T.R., Hussey, R.S., Mitchum, M.G., Davis, E.L. and Baum, T.J.
883 (2008) Cellulose binding protein from the parasitic nematode Heterodera schachtii
884 interacts with Arabidopsis pectin methylesterase: cooperative cell wall modification
885 during parasitism. *Plant Cell*, 20, 3080–93. Available at:
886 http://www.ncbi.nlm.nih.gov/pubmed/19001564 [Accessed February 5, 2019].
887 Hocq, L., Guinand, S., Habrylo, O., et al. (2020) The exogenous application of AtPGLR, an
888 endo-polygalacturonase, triggers pollen tube burst and repair. *Plant J.*, n/a. Available at:
889 https://doi.org/10.1111/tpj.14753.
890 Hocq, L., Pelloux, J. and Lefebvre, V. (2017) Connecting Homogalacturonan-Type Pectin
891 Remodeling to Acid Growth. *Trends Plant Sci.*, 22, 20–29. Available at:
892 http://dx.doi.org/10.1016/j.tplants.2016.10.009.
893 Hocq, L., Sénéchal, F., Lefebvre, V., et al. (2017) Combined Experimental and
894 Computational Approaches Reveal Distinct pH Dependence of Pectin Methylesterase
895 Inhibitors. *Plant Physiol.*, 173, 1075–1093. Available at:
896 http://www.plantphysiol.org/lookup/doi/10.1104/pp.16.01790.
897 Hruz, T., Laule, O., Szabo, G., Wessendorp, F., Bleuler, S., Oertle, L., Widmayer, P.,
898 Gruissem, W. and Zimmermann, P. (2008) Genevestigator V3: A Reference Expression
899 Database for the Meta-Analysis of Transcriptomes Y. Van de Peer, ed. *Adv.*
900 *Bioinformatics*, 2008, 420747. Available at: https://doi.org/10.1155/2008/420747.
901 Johansson, K., El-Ahmad, M., Friemann, R., Jörnvall, H., Markovič, O. and Eklund, H.
902 (2002) Crystal structure of plant pectin methylesterase. *FEBS Lett.*, 514, 243–249.
903 Jolie, R.P., Duvetter, T., Loey, A.M. Van and Hendrickx, M.E. (2010) Pectin methylesterase
904 and its proteinaceous inhibitor: A review. *Carbohydr. Res.*, 345, 2583–2595.
905 Kent, L.M., Loo, T.S., Melton, L.D., Mercadante, D., Williams, M.A.K. and Jameson, G.B.
906 (2016) Structure and properties of a non-processive, salt-requiring, and acidophilic
907 pectin methylesterase from aspergillus Niger provide insights into the key determinants
908 of processivity control. *J. Biol. Chem.*, 291, 1289–1306.
909 Kumpf, R.P., Shi, C.-L., Larrieu, A., Sto, I.M., Butenko, M.A., Peret, B., Riiser, E.S.,
910 Bennett, M.J. and Aalen, R.B. (2013) Floral organ abscission peptide IDA and its
911 HAE/HSL2 receptors control cell separation during lateral root emergence. *Proc. Natl.*
912 *Acad. Sci.*, 110, 5235–5240. Available at:

913 http://www.pnas.org/cgi/doi/10.1073/pnas.1210835110.
914 Leroux, C., Bouton, S., Kiefer-Meyer, M.-C., et al. (2015) PECTIN METHYLESTERASE48
915 Is Involved in Arabidopsis Pollen Grain Germination. *Plant Physiol.*, 167, 367–380.
916 Available at: http://www.plantphysiol.org/lookup/doi/10.1104/pp.114.250928.
917 Lin, T.-P., Liu, C.-C., Chen, S.-W. and Wang, W.-Y. (1989) Purification and
918 Characterization of Pectinmethylesterase from Ficus awkeotsang Makino Achenes .
919 *Plant Physiol.*, 91, 1445–1453.
920 Malamy, J.E. and Benfey, P.N. (1997) <Malamy benfey paper.pdf>. , 44, 33–44.
921 Markovič, O. and Janeček, Š. (2004) Pectin methylesterases: Sequence-structural features and
922 phylogenetic relationships. *Carbohydr. Res.*, 339, 2281–2295.
923 Markovič, O. and Kohn, R. (1984) Mode of pectin deesterification by Trichoderma reesei
924 pectinesterase. *Experientia*, 40, 842–843.
925 Mercadante, D., Melton, L.D., Jameson, G.B. and Williams, M.A.K. (2014) Processive pectin
926 methylesterases: the role of electrostatic potential, breathing motions and bond cleavage
927 in the rectification of Brownian motions. *PLoS One*, 9, e87581. Available at:
928 http://www.ncbi.nlm.nih.gov/pubmed/24503943 [Accessed June 5, 2020].
929 Mercadante, D., Melton, L.D., Jameson, G.B., Williams, M.A.K. and Simone, A. De (2013)
930 Substrate dynamics in enzyme action: Rotations of monosaccharide subunits in the
931 binding groove are essential for pectin methylesterase processivity. *Biophys. J.*, 104,
932 1731–1739. Available at: http://dx.doi.org/10.1016/j.bpj.2013.02.049.
933 Micheli, F. (2001) Pectin methylesterases: Cell wall enzymes with important roles in plant
934 physiology. *Trends Plant Sci.*, 6, 414–419.
935 Milani, P., Gholamirad, M., Traas, J., Arnéodo, A., Boudaoud, A., Argoul, F. and Hamant, O.
936 (2011) In vivo analysis of local wall stiffness at the shoot apical meristem in Arabidopsis
937 using atomic force microscopy. *Plant J.*, 67, 1116–1123.
938 Nguyen-Kim, H., San Clemente, H., Balliau, T., Zivy, M., Dunand, C., Albenne, C. and
939 Jamet, E. (2016) *Arabidopsis thaliana* root cell wall proteomics: Increasing the proteome
940 coverage using a combinatorial peptide ligand library and description of unexpected Hyp
941 in peroxidase amino acid sequences. *Proteomics*, 16, 491–503. Available at:
942 http://doi.wiley.com/10.1002/pmic.201500129 [Accessed May 22, 2019].
943 Peaucelle, A., Braybrook, S.A., Le Guillou, L., Bron, E., Kuhlemeier, C. and Höfte, H. (2011)
944 Pectin-Induced Changes in Cell Wall Mechanics Underlie Organ Initiation in
945 Arabidopsis. *Curr. Biol.*, 21, 1720–1726. Available at:
946 http://www.sciencedirect.com/science/article/pii/S0960982211009638.

947 Peaucelle, A., Louvet, R., Johansen, J.N., et al. (2011) The transcription factor
948 BELLRINGER modulates phyllotaxis by regulating the expression of a pectin
949 methylesterase in Arabidopsis. *Development*, 138, 4733–4741.
950 Peaucelle, A., Louvet, R., Johansen, J.N., Höfte, H., Laufs, P., Pelloux, J. and Mouille, G.
951 (2008) Arabidopsis phyllotaxis is controlled by the methyl-esterification status of cell-
952 wall pectins. *Curr. Biol.*, 18, 1943–8. Available at:
953 http://www.ncbi.nlm.nih.gov/pubmed/19097903.
954 Peaucelle, A., Wightman, R. and Höfte, H. (2015) The Control of Growth Symmetry
955 Breaking in the Arabidopsis Hypocotyl. *Curr. Biol.*, 25, 1746–1752.
956 Pelletier, S., Orden, J. Van, Wolf, S., et al. (2010) A role for pectin de-methylesterification in
957 a developmentally regulated growth acceleration in dark-grown Arabidopsis hypocotyls.
958 *New Phytol.*, 188, 726–739.
959 Pelloux, J., Rustérucci, C. and Mellerowicz, E.J. (2007) New insights into pectin
960 methylesterase structure and function. *Trends Plant Sci.*, 12, 267–277.
961 Peng, C.C., Hsiao, E.S.L., Ding, J.L.C. and Tzen, J.T.C. (2005) Functional expression in
962 Pichia pastoris of an acidic pectin methylesterase from jelly fig (Ficus awkeotsang). *J.*
963 *Agric. Food Chem.*, 53, 5612–5616.
964 Refrégier, G., Pelletier, S., Jaillard, D. and Höfte, H. (2004) Interaction between wall
965 deposition and cell elongation in dark-grown hypocotyl cells in Arabidopsis. *Plant*
966 *Physiol.*, 135, 959–968.
967 Ren, C. and Kermode, A.R. (2000) An increase in pectin methyl esterase activity
968 accompanies dormancy breakage and germination of yellow cedar seeds. *Plant Physiol.*,
969 124, 231–242. Available at: /pmc/articles/PMC59138/?report=abstract [Accessed June
970 30, 2020].
971 Ridley, B.L., O'Neill, M.A. and Mohnen, D. (2001) Pectins: Structure, biosynthesis, and
972 oligogalacturonide-related signaling. *Phytochemistry*, 57, 929–967. Available at:
973 https://pubmed.ncbi.nlm.nih.gov/11423142/ [Accessed November 5, 2020].
974 Salamin, K., Sriranganadane, D., Léchenne, B. and Jousson, O. (2010) Endogenous Secreted
975 Subtilisin in Pichia pastoris GS115 and KM71 Strains 1 2. Available at:
976 http://aem.asm.org/ [Accessed June 11, 2020].
977 San Clemente, H. and Jamet, E. (2015) WallProtDB, a database resource for plant cell wall
978 proteomics. *Plant Methods*, 11, 1–7.
979 Savary, B.J. (2001) Perfusion chromatography separation of the tomato fruit-specific pectin
980 methylesterase from a semipurified commercial enzyme preparation. *Prep. Biochem.*

Biotechnol., 31, 241–258.

Savary, B.J., Vasu, P., Cameron, R.G., McCollum, T.G. and Nuñez, A. (2013) Structural Characterization of the Thermally Tolerant Pectin Methylesterase Purified from Citrus sinensis Fruit and Its Gene Sequence. *J. Agric. Food Chem.*, 61, 12711–12719. Available at: https://doi.org/10.1021/jf403914u.

Savary, B.J., Vasu, P., Nunez, A. and Cameron, R.G. (2010) Identification of thermolabile pectin methylesterases from sweet orange fruit by peptide mass fingerprinting. *J. Agric. Food Chem.*, 58, 12462–12468.

Sénéchal, F., Graff, L., Surcouf, O., et al. (2014) Arabidopsis PECTIN METHYLESTERASE17 is co-expressed with and processed by SBT3.5, a subtilisin-like serine protease. *Ann. Bot.*, 114, 1161–1175.

Sénéchal, F., L'Enfant, M., Domon, J.M., et al. (2015) Tuning of pectin methylesterification: Pectin methylesterase inhibitor 7 modulates the processive activity of co-expressed pectin methylesterase 3 in a pH-dependentmanner. *J. Biol. Chem.*, 290, 23320–23335.

Sénéchal, F., Wattier, C., Rustérucci, C. and Pelloux, J. (2014) Homogalacturonan-modifying enzymes: Structure, expression, and roles in plants. *J. Exp. Bot.*, 65, 5125–5160.

Søndergaard, C.R., Olsson, M.H.M., Rostkowski, M. and Jensen, J.H. (2011) Improved treatment of ligands and coupling effects in empirical calculation and rationalization of p K a values. *J. Chem. Theory Comput.*, 7, 2284–2295. Available at: https://pubmed.ncbi.nlm.nih.gov/26606496/ [Accessed November 24, 2020].

Swarup, K., Benková, E., Swarup, R., et al. (2008) The auxin influx carrier LAX3 promotes lateral root emergence. *Nat. Cell Biol.*, 10, 946–954.

Thonar, C., Liners, F. and Cutsem, P. Van (2006) Polymorphism and modulation of cell wall esterase enzyme activities in the chicory root during the growing season. *J. Exp. Bot.*, 57, 81–89. Available at: http://academic.oup.com/jxb/article/57/1/81/442028/Polymorphism-and-modulation-of-cell-wall-esterase [Accessed January 6, 2020].

Voxeur, A., Habrylo, O., Guénin, S., et al. (2019) Oligogalacturonide production upon Arabidopsis thaliana-Botrytis cinerea interaction. *Proc. Natl. Acad. Sci. U. S. A.*, 116, 19743–19752.

Wachsman, G., Zhang, J., Moreno-Risueno, M.A., Anderson, C.T. and Benfey, P.N. (2020) Cell wall remodeling and vesicle trafficking mediate the root clock in Arabidopsis. *Science*, 370, 819–823.

Wade, R.C., Gabdoulline, R.R. and Rienzo, F. De (2001) Protein interaction property similarity analysis. *Int. J. Quantum Chem.*, 83, 122–127. Available at:

http://doi.wiley.com/10.1002/qua.1204 [Accessed November 17, 2020].

Wang, J., Cieplak, P. and Kollman, P.A. (2000) *How Well Does a Restrained Electrostatic Potential (RESP) Model Perform in Calculating Conformational Energies of Organic and Biological Molecules? Keywords: additive force field; nonadditive force field; restrained electrostatic potential (RESP); torsional angle parameterization*, Available at: www.amber.ucsf.edu/amber/ [Accessed November 24, 2020].

Wang, X., Wilson, L. and Cosgrove, D.J. (2020) Pectin methylesterase selectively softens the onion epidermal wall yet reduces acid-induced creep. *J. Exp. Bot.*, 71, 2629–2640. Available at: https://pubmed.ncbi.nlm.nih.gov/32006044.

Willats, W.G.T., Knox, J.P. and Mikkelsen, J.D. (2006) Pectin: New insights into an old polymer are starting to gel. *Trends Food Sci. Technol.*, 17, 97–104.

Willats, W.G.T., Orfila, C., Limberg, G., et al. (2001) Modulation of the degree and pattern of methyl-esterification of pectic homogalacturonan in plant cell walls: Implications for pectin methyl esterase action, matrix properties, and cell adhesion. *J. Biol. Chem.*, 276, 19404–19413.

Wolf, S., Rausch, T. and Greiner, S. (2009) The N-terminal pro region mediates retention of unprocessed type-I PME in the Golgi apparatus. *Plant J.*, 58, 361–375.

Figures

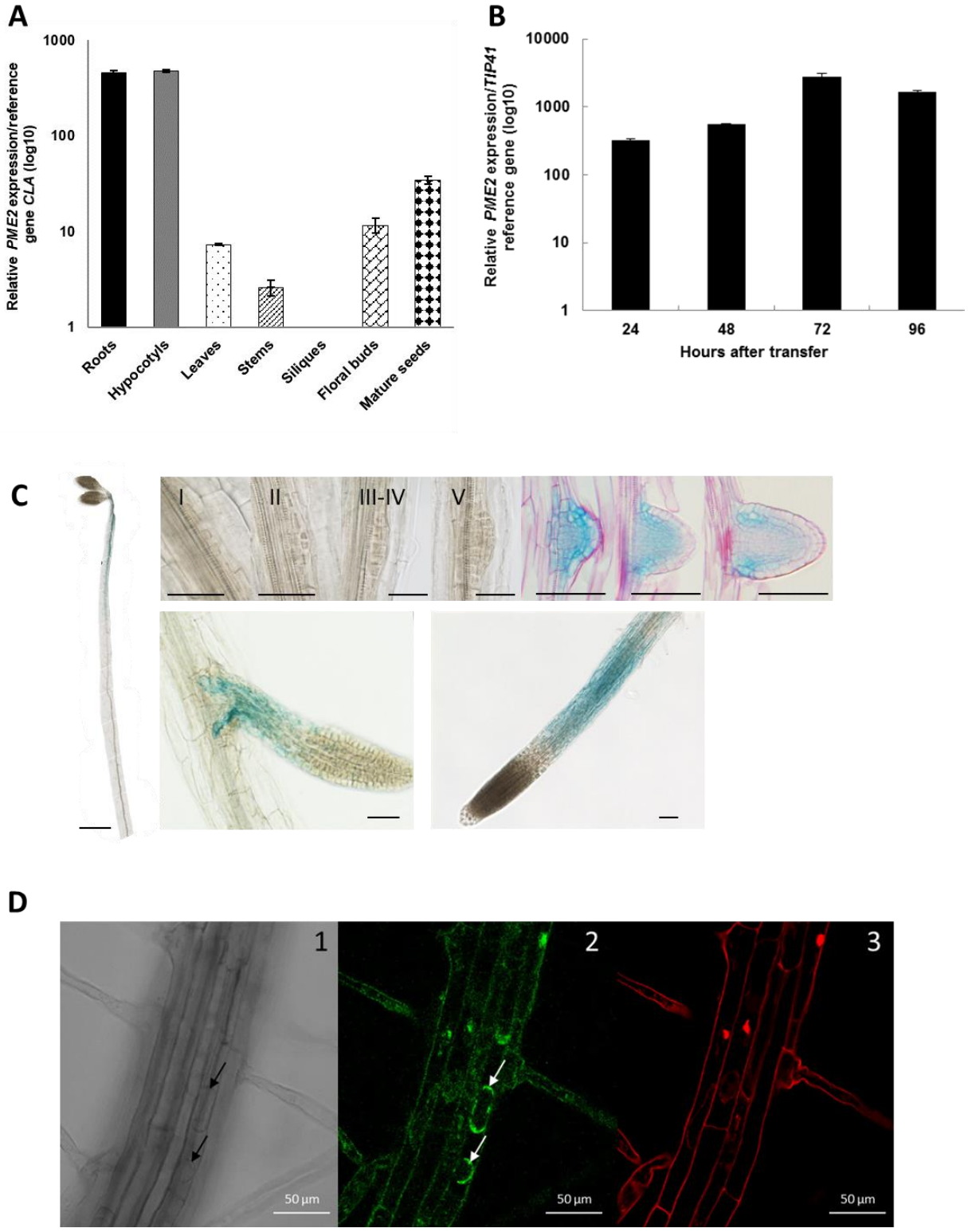

Figure 1: *AtPME2* gene is highly expressed in roots and dark-grown hypocotyls and targeted at the cell wall

At*PME2* gene expression was quantified **(A)** on different organs and quantified using *CLATHRIN* (*At5g46630*) as a reference gene, **(B)** on various stages of dark-grown hypocotyl elongation (up to 96h post-induction) and quantified using *TIP41* (*At4G34270*) as a reference gene and (**C**) Localization of AtPME2 promotor activity during in 4 day-old dark-grown

hypocotyl (left, scale bar: 1 mm) and lateral root initiation (right, scale bars: 100 µm). (**D**) Subcellular localization of the AtPME2 protein. Arabidopsis plants were transformed with Rhizobium radiobacter containing a 35S::AtPME2-GFP construct and GFP fluorescence was imaged in 6-day old roots under confocal microscope. 1. Brightfield imaging of plasmolyzed root cells, 2. AtPME2-GFP fused protein signal, 3. Propidium iodide staining of the cell walls. Scale bar: 50 µm; Arrows indicate retraction of the tonoplast due to plasmolysis.

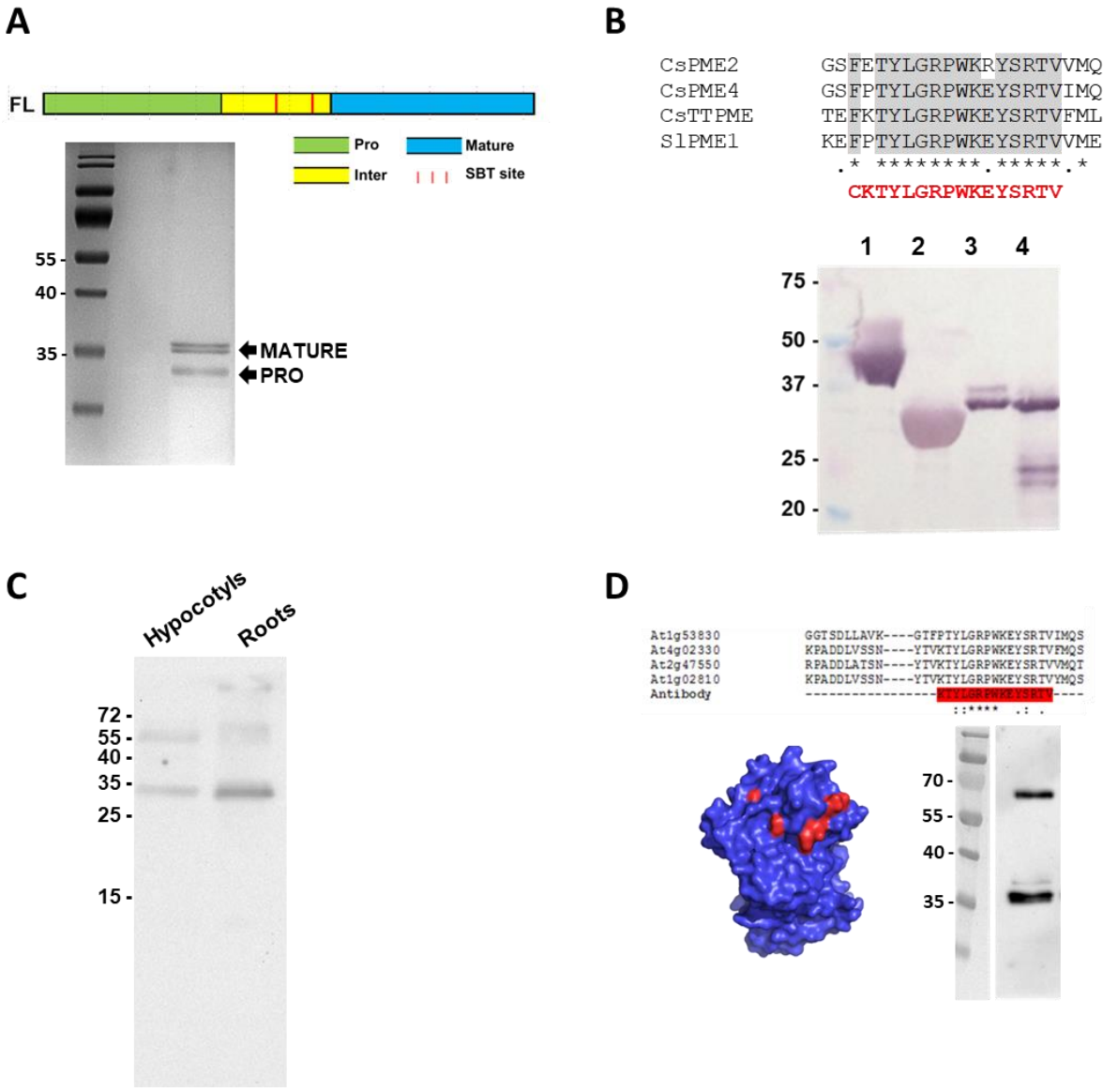

Figure 2: AtPME2 is effectively produced in *Pichia pastoris*

(**A**) *At*PME2 mature protein recovered from *Pichia pastoris* culture supernatant (purified by ion exchange chromatography) was separated by SDS-PAGE (Coomassie-Blue stained gel). Closely related bands at a MW ~35 kDa represent the two forms of processed enzymes (see scheme of protein structure above, including processing motifs). The lower band represent the PRO part. **(B)** Design of a peptide antibody that can detect sweet orange and tomato PME isoforms. The generic anti PME antibody was designed on a highly conserved part of the mature protein (see alignment). Western blot analysis allowed detection of purified PMEs, 1: CsTT-PME (*Citrus sinensis* thermally-tolerant isozyme; (Savary *et al.*, 2013)), 2: CsPME2 (*C. sinensis* fruit-specific salt-independent isozyme, (Savary *et al.*, 2010), 3: CsPME4 (*C. sinensis* salt-dependent isozyme, (Savary *et al.*, 2010)), and SlPME1 (*Solanum lycopersicum* isozyme (Savary, 2001). **(C)** Western blot analysis of cell- wall-enriched protein extracts from 7 day-old roots and 4 day-old dark grown hypocotyls using the anti PME antibody. Both processed and non-processed forms of PME can be detected. **(D)** Western blot detection of AtPME2 purified by cation-exchange chromatography from concentrated *Pichia* culture media.

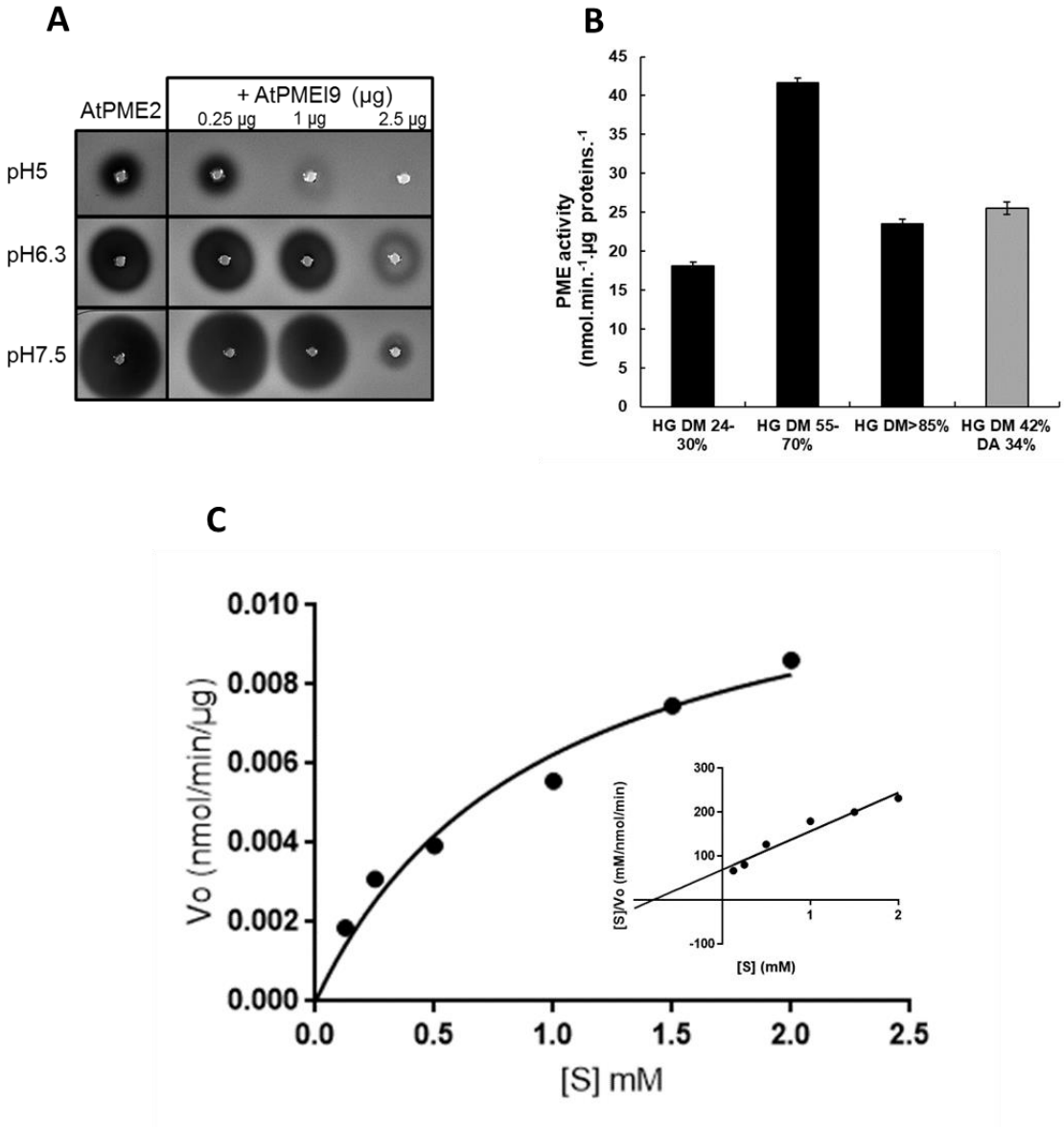

Figure 3: AtPME2 is active and can be inhibited by PMEI

(**A**) pH-dependence of AtPME2 activity. Activity of purified AtPME2 was assessed at three distinct pH (5, 6.3 and 7.5) with increasing quantities of the pH-independent AtPMEI9. Activity was determined with the gel diffusion assay using pectins DM 85% as a substrate and ruthenium red staining. The diameter of the halo reflects PME activity. (**B**) Substrate specificity of AtPME2. Activity of purified AtPME2 on pectic substrates with increasing degree of methylesterification (DM) was determined at an optimal pH of 7.5. Data represent the mean ± SE of three to five replicates. HG: Homogalacturonan, DA: Degree of acetylation. (**C**) Determination of Km and Vmax for AtPME2. Activity was assessed using various concentrations of pectins DM 55-10% at 37°C and pH 7.5.

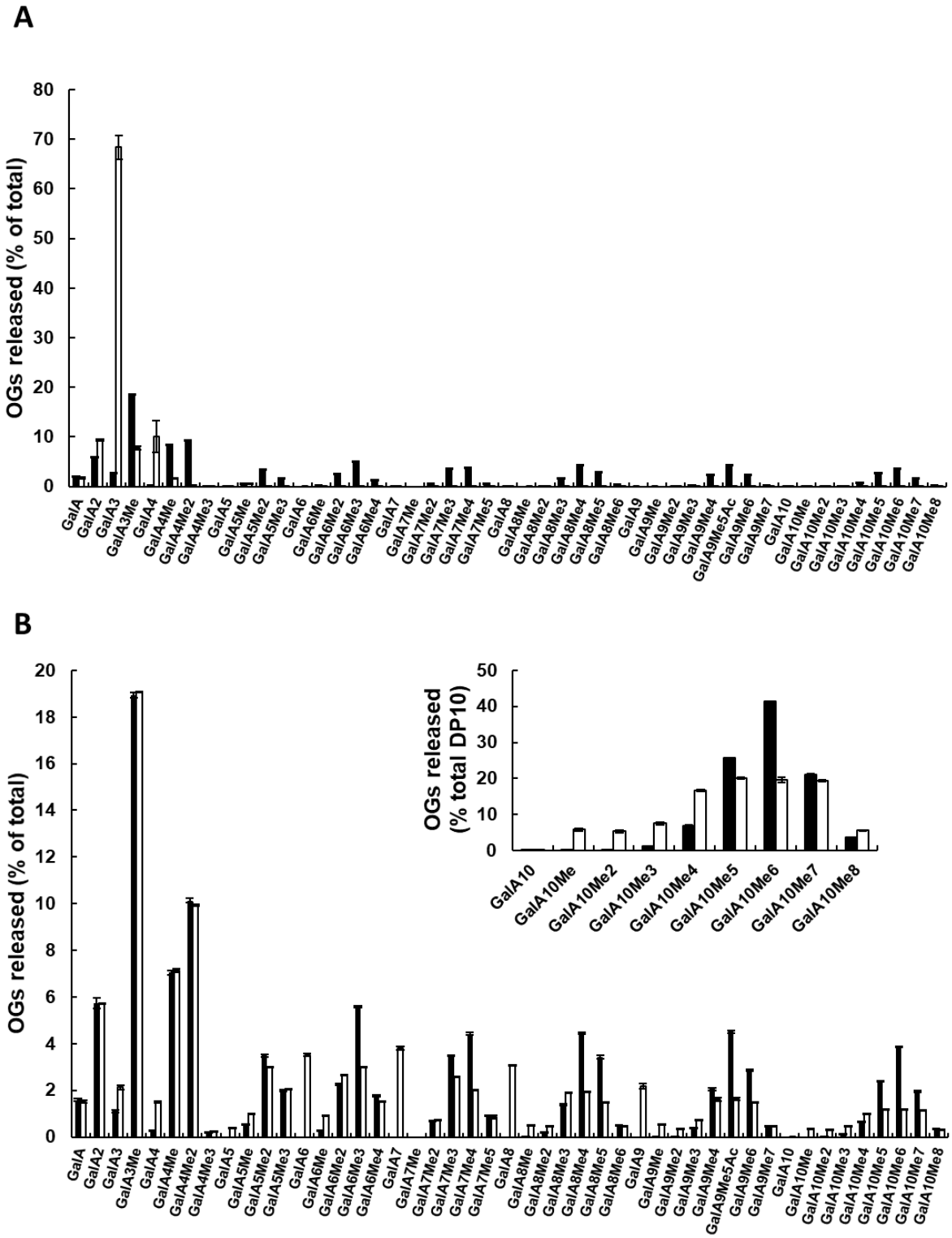

Figure 4: Determination of AtPME2 mode of action using an LC-MS/MS

Comparisons of the oligogalacturonides (OGs) produced following demethylesterification by AtPME2 at (**A**) pH 8 and (**B**) pH 5. A population of OGs of various degree of polymerization (DP) and degree of methylesterification (DM) was first generated by action of *Aspergillus aculeatus* polygalacturonase during 2 h at 40°C. After heat denaturation of the PGs, the OGs were incubated overnight at 40°C with buffer (black bars) or isoactivities of AtPME2 at pH 5

1085 and pH 8 (white bars). OGs were separated using SEC and analyzed using MS/MS. Data
1086 represent the mean ± SE of three replicates.
1087

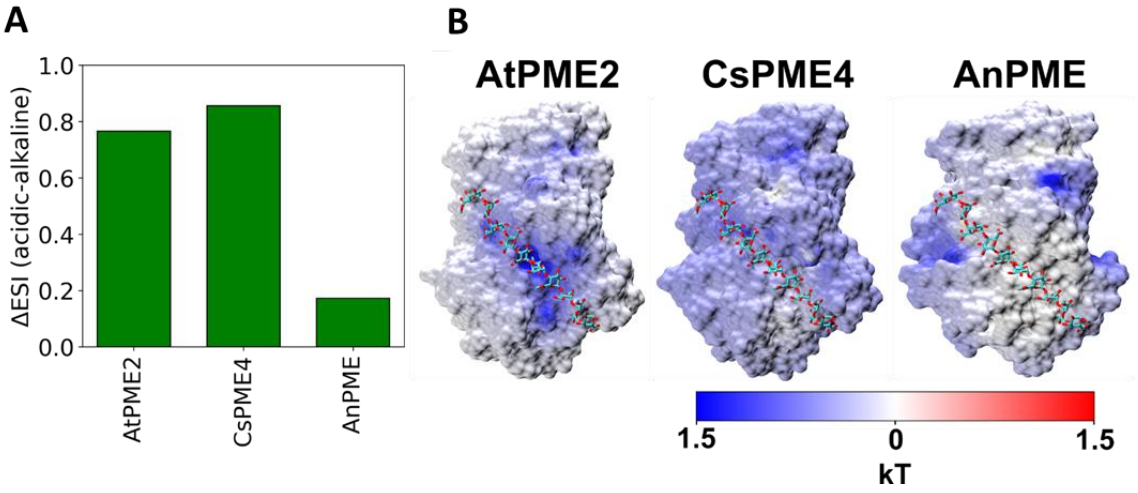

Figure 5: Electrostatic potential of AtPME2 is pH-dependent
(A) Difference between the electrostatic similarity indices of AtPME2, CsPME4 and AnPME at pH 5.0 (acidic) and pH 8.0 (basic). **(B)** Electrostatic potentials of the three PME isoforms projected on the protein surfaces. The electrostatic potentials are the resultant of the subtraction between the electrostatic potentials obtained at pH 8.0 from the one obtained at pH 5.0 for each protein. The potentials of AnPME and CsPME4 have been then divided by the electrostatic potential of AtPME2 to better show the comparison with AtPME2.

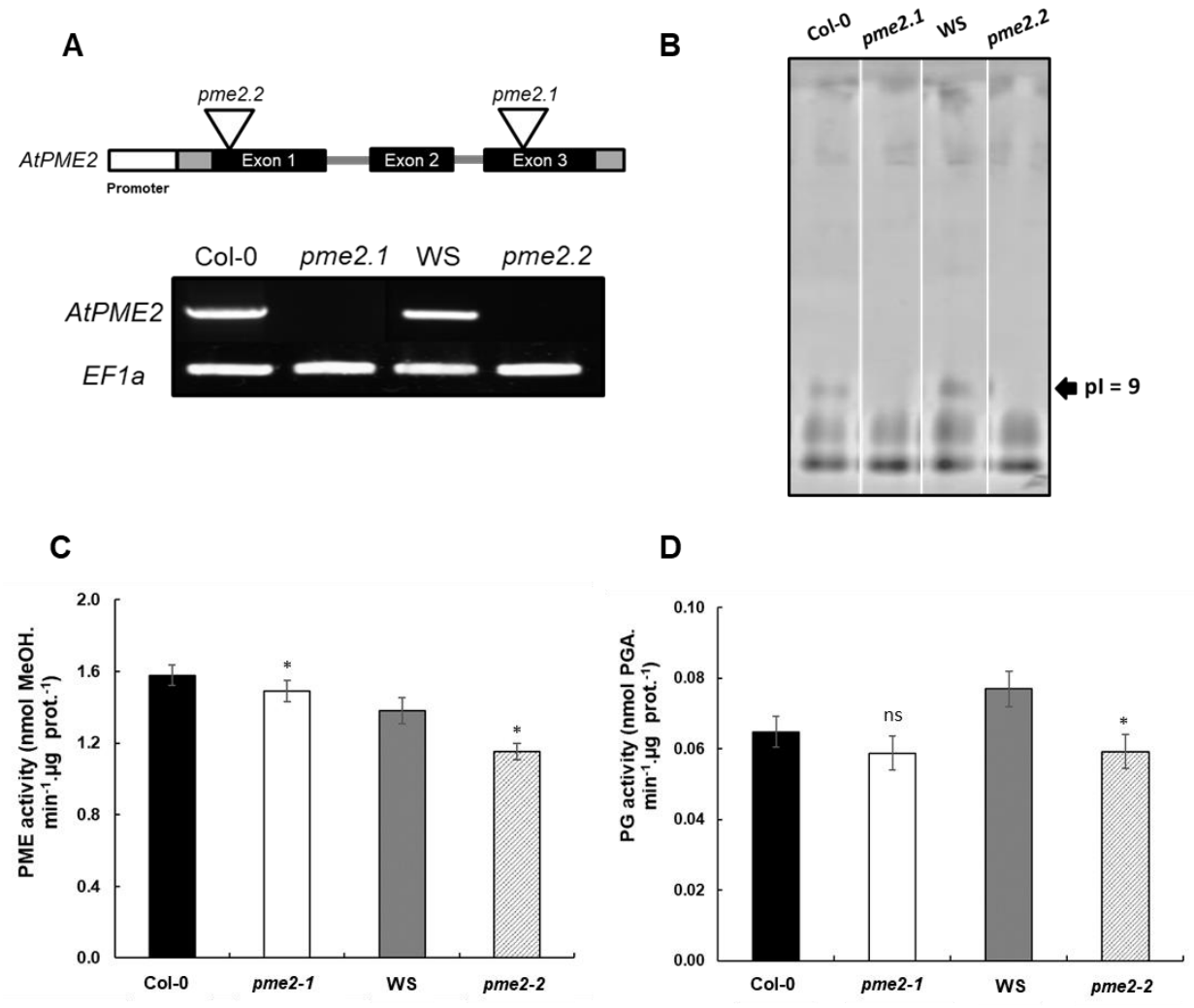

Figure 6: Defect in AtPME2 leads changes in pectin remodeling enzyme activities

(A) Schematic representation of *AtPME2* gene structure and localisation of the T-DNA insertions for *pme2-1* (GK-835A09, in the third exon) and *pme2-2* (FLAG_445B05, in the first exon). PCR analysis of *pme2-1*, *pme2-2* and WT (Col-0 and WS) hypocotyl cDNAs using specific primers flanking the T-DNA insertion sites. *EF1α* was used as reference gene. (**B**) Isoelectric focusing (IEF) of cell wall-enriched protein extracts from 4 day-old dark-grown hypocotyls of wild type Col-0/WS and *pme2-1/pme2-2* mutants. The same PME activities (15 mU) were loaded for each genotype. PME isoforms were separated and zymogram of PME activity was performed by incubating the gel with pectins (DM > 85 %), followed by ruthenium red staining. Similar observations were obtained from two independent experiments. Black arrow indicates the disappearance of an activity at a pI ~9 in *pme2* mutants. (**C**) Total PME activity of cell wall-enriched protein extracts from 4 day-old dark-grown hypocotyls of wild type Col-0/WS and *pme2-1/pme2-2* mutants. Data represent the means of PME activity in nmol of methanol.min^{-1}/µg of protein^{-1}± SE of three independent protein extractions and three technical replicates (n=9). (**D**) Total PG activity of cell wall-enriched protein extracts from 4 day-old dark-grown hypocotyls of wild type Col-0/WS and *pme2-1/pme2-2* mutants. Data represent the means of PG activity in nmol of PGA.min^{-1}/µg of protein^{-1} ± SE of three independent protein extractions and three technical replicates (n=9). Significant differences ($p<0.05$*) were determined according to Wilcoxon test. Non-significant differences are indicated with ns.

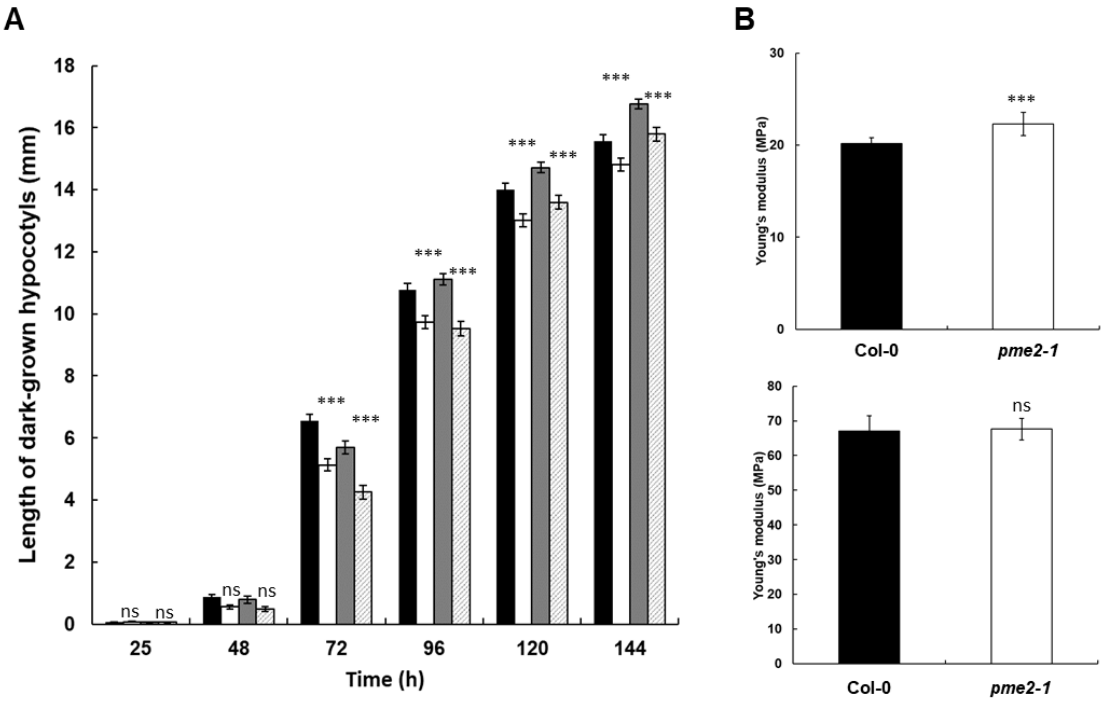

Figure 7: Defect in AtPME2 leads increased cell wall stiffness and reduced hypocotyl length

(**A**) Growth kinematic analysis of etiolated hypocotyls of wild type Col-0 (black bar), WS (grey bar), *pme2-1* (white bar) and *pme2-2* (hatched bar). Data represent the means of length in mm ± SE (n > 30) for each condition. (**B**) Cell wall stiffness of Col-0 (black bar) and pme2-1 (white bar) assessed by Atomic Force Microscopy on 3 day-old dark-grown hypocotyls at the bottom part (bottom panel) and below the hook (top panel). Significant differences ($p<0.001$***) were determined according to Wilcoxon test. Non-significant differences are indicated with ns.

Supplemental material

Supplemental Figure 1: Identification of peptides mapping the mature part of AtPME2 in cell wall-enriched extracts of Col-0 dark-grown hypocotyls using nano LC-MS/MS. The full length amino-acid sequence is shown, with PRO part in purple, putative processing motifs (RKLK, RRLL) are in green.

A

FL	FL-F	CTGCAGgagccacaacaacaaac
	FL-R	GCGGCCGCaagacttaacgagaaagga
Δ4FL	Δ4FL-F	CTGCAGgaaaccaaaacaaaaaccaa
	Δ4FL-R	GCGGCCGCaagacttaacgagaaagga
Δ8FL	Δ8FL-F	CTGCAGgaaaccaaaaaatcacaactc
	Δ8FL-R	GCGGCCGCaagacttaacgagaaagga
Δ12FL	Δ12FL-F	CTGCAGgaacaactctatcttcgacatca
	Δ12FL-R	GCGGCCGCaagacttaacgagaaagga
Δ16FL	Δ16FL-F	CTGCAGgatcgacatcacacgcc
	Δ16FL-R	GCGGCCGCaagacttaacgagaaagga
Δ20FL	Δ20FL-F	CTGCAGgagccattctaaaatctgtttg
	Δ20FL-R	GCGGCCGCaagacttaacgagaaagga
Δ42FL	Δ42FL-F	CTGCAGgaaccggaggaaaagaga
	Δ42FL-R	GCGGCCGCaagacttaacgagaaagga
Δ115FL	Δ115FL-F	CTGCAGgacctaagcaaaaatctctga
	Δ115FL-R	GCGGCCGCaagacttaacgagaaagga
Δ192FL	Δ192FL-F	CTGCAGgaaagtcttcaaccttcacc
	Δ192FL-R	GCGGCCGCaagacttaacgagaaagga
Δ212FL	Δ212FL-F	CTGCAGgattagacagtgatggatgg
	Δ212FL-R	GCGGCCGCaagacttaacgagaaagga

B

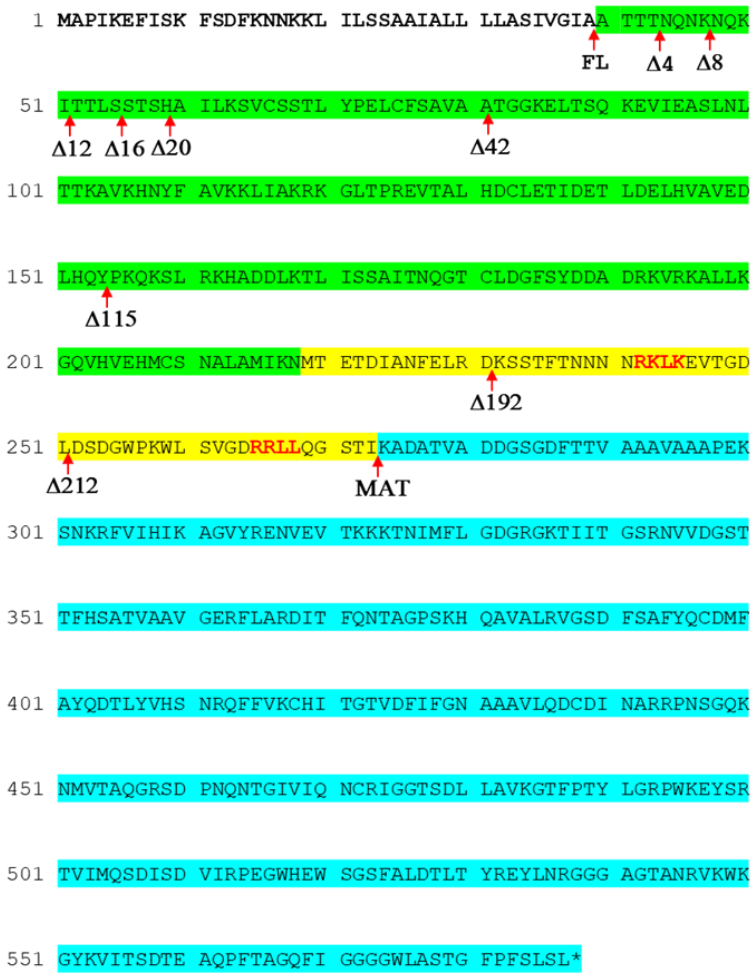

Supplemental Figure 2: (A) Primers used for the amplification of full length AtPME2 sequence and deletion mutants of the PRO part. **(B)** AtPME2 amino-acid sequence highlighting the localization of the sequences used for expression in *Pichia pastoris*.

```
  1 MAPIKEFISK FSDFKNNKKL ILSSAAIALL LLASIVGIAA TTTNQNKNQK
 51 ITTLSSTSHA ILKSVCSSTL YPELCFSAVA ATGGKELTSQ KEVIEASLNL
101 TTKAVKHNYF AVKKLIAKRK GLTPREVTAL HDCLETIDET LDELHVAVED
151 LHQYPKQKSL RKHADDLKTL ISSAITNQGT CLDGFSYDDA DRKVRKALLK
201 GQVHVEHMCS NALAMIKNMT ETDIANFELR DKSSTFTNNN NRKLKEVTGD
251 LDSDGWPKWL SVGDRRLL
                     QG STIKADATVA DDGSGDFTTV AAAVAAAPEK
301 SNKRFVIHIK AGVYRENVEV TKKKTNIMFL GDGRGKTIIT GSRNVVDGST
351 TFHSATVAAV GERFLARDIT FQNTAGPSKH QAVALRVGSD FSAFYQCDMF
401 AYQDTLYVHS NRQFFVKCHI TGTVDFIFGN AAAVLQDCDI NARRPNSGQK
451 NMVTAQGRSD PNQNTGIVIQ NCRIGGTSDL LAVKGTFPTY LGRPWKEYSR
501 TVIMQSDISD VIRPEGWHEW SGSFALDTLT YREYLNRGGG AGTANRVKWK
551 GYKVITSDTE AQPFTAGQFI GGGGWLASTG FPFSLSL
```

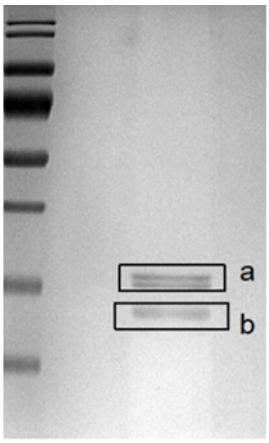

Catalytic region tryptic peptides – 12 observed (2 truncated) ("Band a")

Position	Peptide sequences
75-300	ADATVADDGSGDFTTVAAAVAAAPEK*
316-322	ENVEVTK*
325-334	TNIMFLGDGR
344-363	NVVDGSTTFHSATVAAVGER
368-379	DITFQNTAGPSK
387-412	VGSDFSAFYQCDMFAYQDTL YVHSNR
451-458	NMVTAQGR
459-473	SDPNQNTGIVIQNCR*
474-484	IGGTSDLLAVK*
485-496	GTFPTYLGRPWK*
501-532	TVIMQSDISDVIRPEGWH (+EWSGSFALDTLTYR) – fragment observed
554-587	VITSDTEAQPFTAGQFIGGG (+GWLASTGFPFSLSL) – fragment observed

PRO-region tryptic peptides – 7 observed ("Band b")

Position	Peptide sequences
51-63	ITTLSSTSHAILK
64-85	SVCSSTLYPELCFSAVAATGGK
107-113	HNYFAVK
169-192	TLISSAITNQGTCLDGFSYDDADR
201-217	GQVHVEHMCSNALAMIK
218-230	NMTETDIANFELR
233-242	SSTFTNNNNR

*Peptides observed in cell wall extract and indicated by sequence alignment in Supp Fig 1

Supplemental Figure 3: Identification of peptides mapping the PRO and mature part of AtPME2 following cation exchange purification. Band **a** corresponds to the two proteins at ~35 kDa while band **b** corresponds to the band below ~35kDa (see gel).

A

```
At3g62170          IPDKELEADK----LTIKSYLGRPWKKFATTVIIGTEIGDLIKPEGWTEWQG-EQN--HK
At2g47030          VPDRKLTPER----LTVATYLGRPWKKFSTTVIMSTEMGDLIRPEGWKIWDG-ESF--HK
At2g47040          VPDKKLAAER----LIVESYLGRPWKKFSTTVIINSEIGDVIRPEGWKIWDG-ESF--HK
At2g26450          AANEDLKPVK----EEYKSYLGRPWKNYSRTIIMESKIENVIDPVGWLRWQETDFA--ID
At4g33230          APNEDLKPVK----AQFKSYLGRPWKPHSRTVVMESTIEDVIDPVGWLRWQETDFA--ID
At3g10710          SPLGDLTD--------VMTFLGRPWKNFSTTVIMDSYLHGFIDRKGWLPWTG-DSA--PD
At5g04960          KPLDNLTD--------IQTFLGRPWKDFSTTVIMKSFMDKFINPKGWLPWTG-DTA--PD
At3g10720          KAAPDLAAEP----KSAMTFLGRPWKPYSRTVFMQSYISDIVQPVGWLEWNG-TIG--LD
At5g04970          GAAPDLAADP----KSTMTFLGRPWKPYSRTVYIQSYISDVVQPVGWLEWNG-TTG--LD
At4g03930          TASSDLDTAT------VKTYLGRPWRIFSTVAVLQSFIGDLVDPAGWTPWEG-ETG--LS
At1g11590          TASSDLDTTT------VKTYLGRPWRIFSTVAVMQSFIGDLVDPAGWTPWEG-ETG--LS
At3g27980          TTSSDLDTAT------VKTYLGRPWRRFSTVAVLQSFIGDLVDPAGWTPWKG-ETG--LS
At5g20860          RTDSDLSPVK----HKYSSYLGRPWRKYSRAIVMESYIDDAIAEGGWAGWLD-SGDEVLK
At5g51490          LPAPDLKPVV----GTVKTYMGRPWMKFSRTVVLQTYLDNVVSPVGWSPWIE-GSVFGLD
At5g51500          IPAPDLKPVV----RSVKTYMGRPWMMYSRTVVLKTYIDSVVSPVGWSPWTK-GSTYGLD
At4g15980          TGDASYLPVK----AKNRAFLGRPWKEFSRTIIMNTEIDDVIDPEGWLKWNE-TFA--LN
At3g47400          IAASDLKPVI----RAYKTYLGRPWQAYSRVTIMKTYIDNSISPLGWSPWLR-GSNFALN
At3g14300          SPNGNVT---------ATTYLGRPWKLFSKTVIMQSVIGSFVNPAGWIAWNS-TYDPPPR
At1g23200          ATA-------------SETYLGRPWRSHSRTVFMKCNLGALVSPAGWLPWSG-SFA--LS
At5g64640          NGTEEYMKEFQANPEGHKNFLGRPWKEFSRTVFVNCNLESLISPDGWMPWNG-DFA--LK
At5g53370          LATPDLEASK----GSYPTYLGRPWKLYSRVVYMMSDMGDHIDPRGWLEWNG-PFA--LD
At5g49180          TGEPAYIPVK----SINKAYLGRPWKEFSRTIIMGTTIDDVIDPAGWLPWNG-DFA--LN
At5g09760          NGTEEYMKLFKANPKVHKNFLGRPWKDYSRTVFIGCNLEALITPDGWLPWSG-DFA--LK
At4g02320          LAAPDLIPVQ----ANFKAYLGRPWQLYSRTVIMKSFIDDLVDPAGWLKWKD-DFA--LE
At4g02300          LAAPDLIPVK----ENFKAYLGRPWRKYSRTVIIKSFIDDLIHPAGWLEGKK-DFA--LE
At4g00190          KGAPGVQ--L----GGVKTYLGRPWRSYARTVVIGTYLDTLIEPNGWIDWDN-VTA--LS
At3g49220          LAASDLQATN----GSTQTYLGRPWKLFSRTVYMMSYIGGHVHTRGWLEWNT-TFA--LD
At3g06830          TGDPAYIPMK----SVNKAYLGRPWKEFSRTIIMKTTIDDVIDPAGWLPWSG-DFA--LK
At2g26440          LASEDLFNSS----NKVKSYLGRPWREFSRTVVMESYIDEFIDGSGWSKWNG-GEA--LD
At1g53840          SANGNVI---------APTYLGRPWKEFSTTVIMETVIGAVVRPSGWMSWVS-GVDP-PA
At4g33220          SADADLVPYL----NTTRTYLGRPWKLYSRTVFIRNNMSDVVRPEGWLEWNA-DFA--LD
At3g60730          RAAPEFEAVK----GRFKSYLGRPWKKYSRTVFLKTDIDELIDPRGWREWSG-SYA--LS
At3g43270          AADTDLLLNL----NTTATYLGRPWKLYSRTVFMQNYMSDAINPVGWLEWNG-NFA--LD
At3g05620          LAT-------------QPTYLGRPWKLYSRTVYMNTYMSQLVQPRGWLEWFG-NFA--LD
At3g05610          AGEPDYLAVK----ETSKAYLGRPWKEYSRTIIMNTFIPDFVQPQGWQPWLG-DFG--LK
At2g45220          TAASDLRPVL----GSTKTYLGRPWRQYSRTVFMKTSLDSLIDPRGWLEWDG-NFA--LK
At1g11580          TASSDLAPVK----GSVKTFLGRPWKLYSRTVIMQSFIDNHIDPAGWFPWDG-EFA--LS
At3g14310          GATSDLQSVK----GSFPTYLGRPWKEYSQTVIMQSAISDVIRPEGWSEWTG-TFA--LN
At5g27870          VGEPDYLAVK----EQSKTYLGRPWKEYSRTIIMNTFIPDFVPPEGWQPWLG-EFG--LN
At3g59010          TGS-------------TKTYLGRPWKQYSRTVVMQSFIDGSIHPSGWSPWSS-NFA--LK
At2g43050          TAE-------------SMTYLGRPWKEYSRTVVMQSFIGGSIHPSGWSPWSG-GFG--LK
At1g53830          GGTSDLLAVK----GTFPTYLGRPWKEYSRTVIMQSDISDVIRPEGWHEWSG-SFA--LD
At4g02330          KPADDLVSSN----YTVKTYLGRPWKEYSRTVFMQSYIDEVVEPVGWREWNG-DFA--LS
At2g47550          RPADDLATSN----YTVKTYLGRPWKEYSRTVVMQTYIDGFLEPSGWNAWSG-DFA--LS
At1g02810          KPADDLVSSN----YTVKTYLGRPWKEYSRTVYMQSYIDGFVEPVGWREWNG-DFA--LS
Antibody           ----------------KTYLGRPWKEYSRTV----------------------------
                                  ::****  .: .
```

B

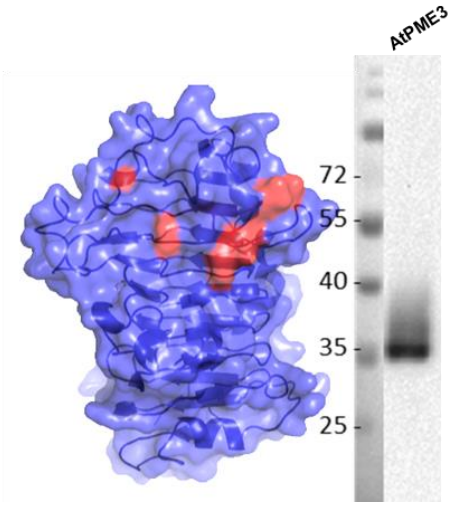

Supplemental Figure 4: (A) Sequence alignment of 45 Arabidopsis PME isoforms showing the conservation of the epitope used for production of the generic anti-PME antibody. **(B)** Immunodetection of AtPME3 using the generic anti-PME antibody

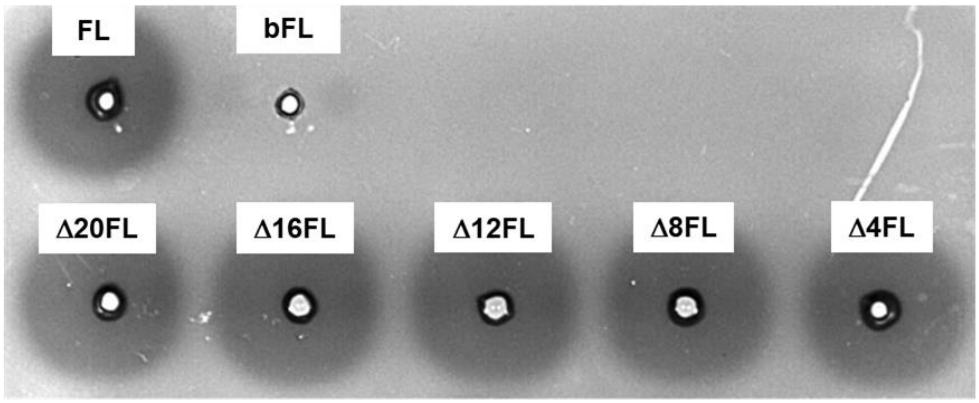

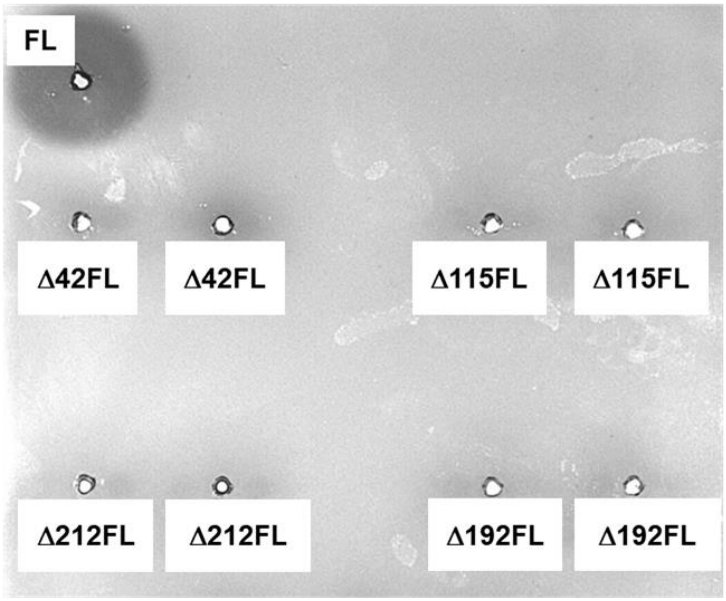

Deletion	FL	Δ4FL	Δ8FL	Δ12FL	Δ16FL	Δ20FL	Δ42FL	Δ115FL	Δ192FL	Δ212FL
Activity	+	+	+	+	+	+	-	-	-	-

Supplemental Figure 5: Effects of deletion of the N-terminus sequence of AtPME2 on the production of an active enzyme in Pichia. F: Full length AtPME2, FLb: heat-denaturated AtPME2, Δ4FL to Δ212FL: Deletion of 4 to 212 amino acids of the PRO part. PME activity was assessed on concentrated supernatants using gel diffusion assay.

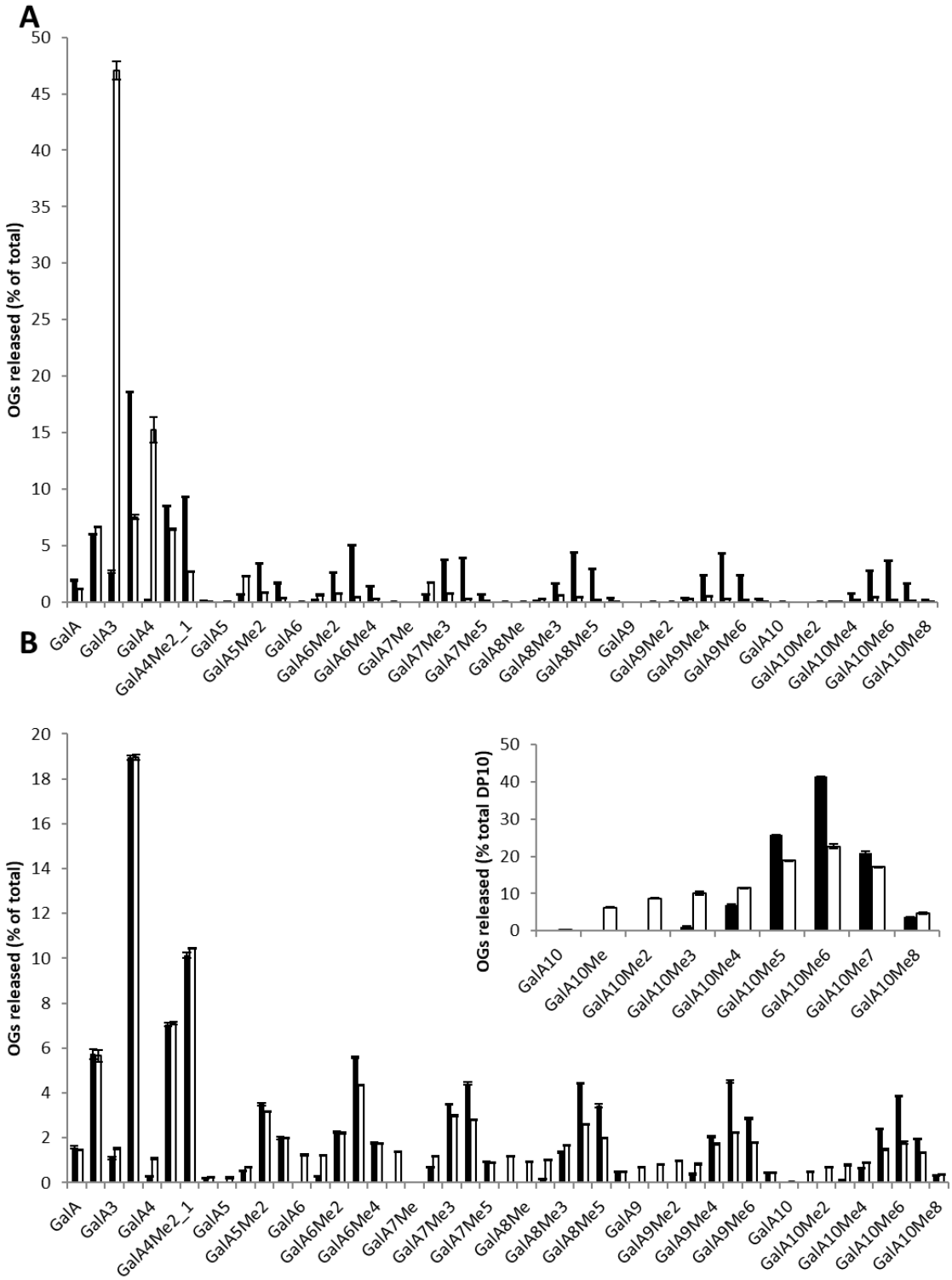

Supplemental Figure 6: Determination of the processivity of CsPME at **(A)** pH 8 and (**B**) pH 5 using LC-MS/MS. Non-digested samples (black bars); CsPME digestion (white bars). Data represent the mean ± SE of three replicates.

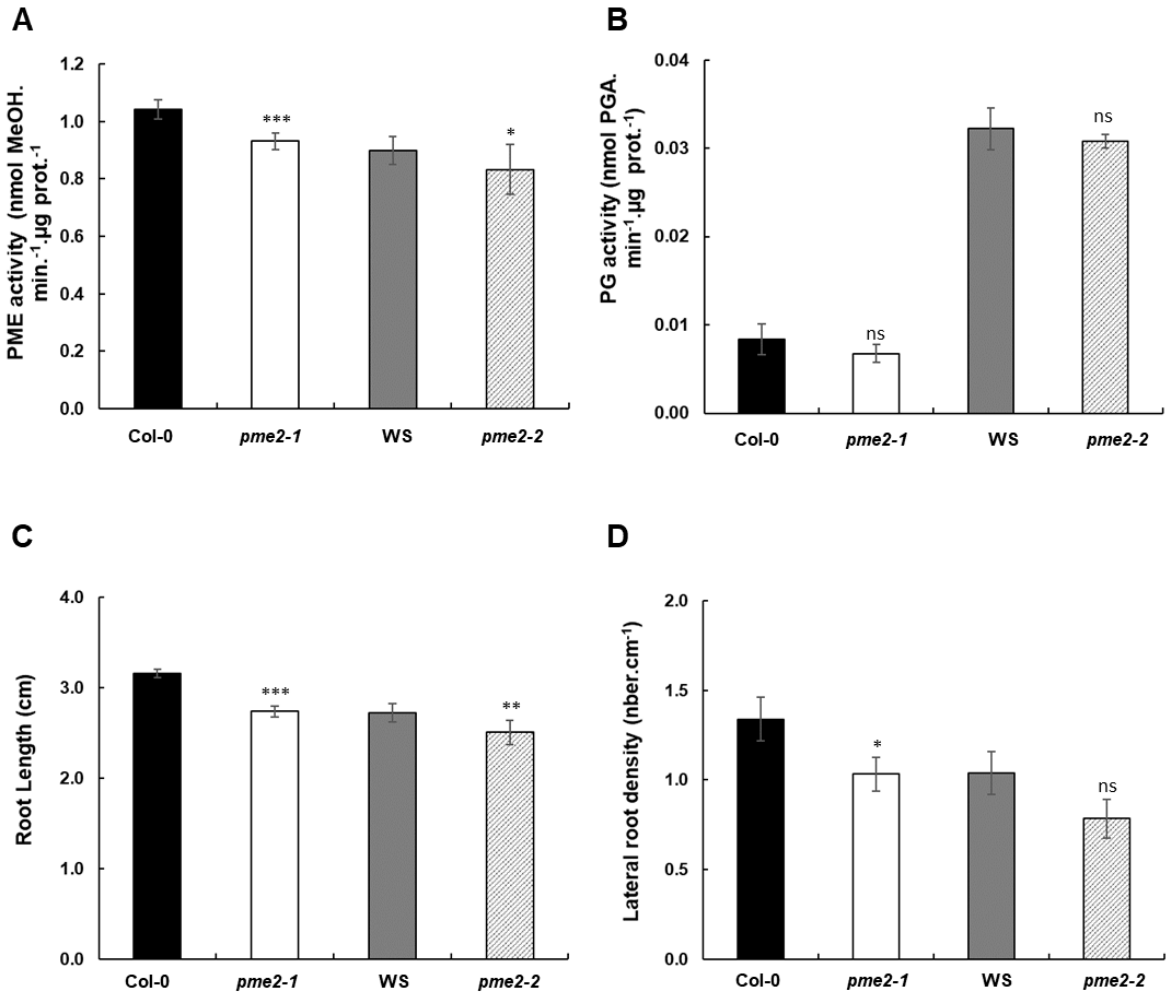

Supplemental Figure 7: *pme2* mutation affect root development. **(A**) Total PME activity of cell wall-enriched protein extracts from 7-day-old roots of wild type Col-0/WS and *pme2-1/pme2-2* mutants. Data represent the means of PME activity in nmol of methanol.min^{-1}/µg of protein^{-1}± SE of three independent protein extractions and three technical replicates (n=9). (**B**) Total PG activity of cell wall-enriched protein extracts from 4 day-old dark-grown hypocotyls of wild type Col-0/WS and *pme2-1/pme2-2* mutants. Data represent the means of PG activity in nmol of PGA.min^{-1}/µg of protein^{-1} ± SE of three independent protein extractions and three technical replicates (n=9). **(C)** Root length measured on 7-day-old roots of wild-type and *pme2-1* and *pme2-2* mutant lines (n>90). **(D)** Lateral root density (number of emerged lateral root.cm-1) of wild-type and *pme2-1* and *pme2-2* mutant lines (n>90). Statistical analyses were realized using Mann-Whitney test: * P<0.05.

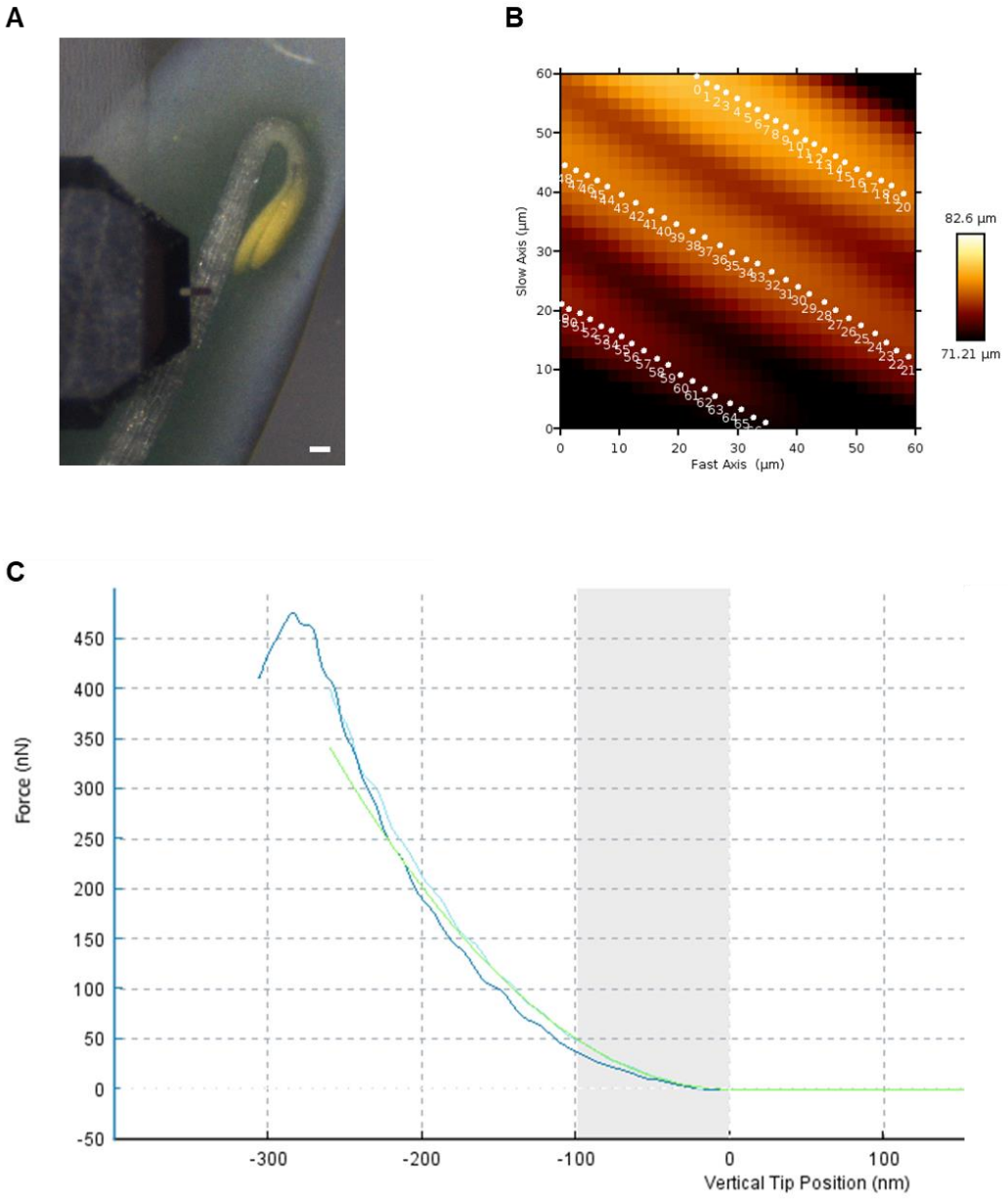

Supplemental Figure 8: AFM analysis of 3-day-old hypocotyls. **(A)** Top view of a wild-type hypocotyl under the atomic force microscope; the cantilever (rectangular with a triangular end) is located over the hypocotyl at about 1mm from the hook. Scale bar 100 µm. **(B)** Topographic image of a 60 µm x 60 µm region of the hypocotyl (height scale on right), with three cells partially visible. The white dots show points where force-depth curves were obtained in order to characterise cell wall stiffness. **(C)** Typical force-depth curve with approach in light blue, retract in dark blue. The green curve is a fit of the approach to the Sneddon model, which yields the apparent Young's modulus.

Supplemental Table

A

		Col		*pme2.1*		WS		*pme2.2*	
		% coverage	Nb peptides	% coverage	Nb peptides	% coverage	Nb peptides	% coverage	Nb peptides
AT1G01900.1	Subtilase family protein	18.6	11	14.08	8	10.85	5	13.05	7
AT1G20160.2	Subtilisin-like serine endopeptidase protein	12.88	8	15.34	9	14.25	9	14.25	9
AT1G53830.1	Pectin methylesterase 2	19.08	5			18.57	5		
AT2G05920.1	Subtilase family protein	26.92	16	31.03	17	32.36	17	31.03	16
AT2G43050.1	Plant invertase/pectin methylesterase inhibitor	25.68	10	27.22	11	22.78	9	18.73	7
AT2G46930.1	Pectinacetylesterase family protein	17.55	5	29.09	8	31.49	9	31.01	8
AT3G05910.1	Pectinacetylesterase family protein	27.95	7	5.54	2	35.42	9	26.75	7
AT3G06770.2	Pectin lyase-like superfamily protein	15.02	5	8.22	2	10.34	3	12.47	4
AT3G07010.1	Pectin lyase-like superfamily protein	10.82	4	10.1	3				
AT3G09410.3	Pectinacetylesterase family protein					6.06	2	8.67	3
AT3G14067.1	Subtilase family protein	24.45	12	24.45	12	26	12	22.91	11
AT3G14310.1	Pectin methylesterase 3	27.87	11	26.52	13	28.04	11	28.04	14
AT3G16850.1	Pectin lyase-like superfamily protein	28.57	7	32.75	9	28.57	8	30.33	8
AT3G43270.1	Plant invertase/pectin methylesterase inhibitor	15.37	5	13.47	4	13.47	4	11.2	3
AT3G49220.1	Plant invertase/pectin methylesterase inhibitor	9.2	5	10.37	6	12.04	7	10.87	7
AT3G55140.2	Pectin lyase-like superfamily protein	7.82	2	11.4	3	7.82	2	10.75	3
AT3G57790.1	Pectin lyase-like superfamily protein	4.69	2	10	5	12.65	6	10	5
AT3G59010.1	Pectin methylesterase 61					15.88	4	13.04	4
AT3G61490.1	Pectin lyase-like superfamily protein							11.97	3
AT4G19410.1	Pectinacetylesterase family protein	51.41	12	53.2	9	58.31	13	59.85	13
AT4G23820.1	Pectin lyase-like superfamily protein	32.66	10	10.14	3	18.24	5	9.23	2
AT4G25260.1	Plant invertase/pectin methylesterase inhibitor	26.87	4	40.3	6	32.34	6	23.38	4
AT4G33220.1	Pectin methylesterase 44	19.43	6	19.24	7	19.05	5	16.76	5
AT5G20740.1	Plant invertase/pectin methylesterase inhibitor					11.71	2	11.71	2
AT5G45280.2	Pectinacetylesterase family protein	71.1	16	66.24	13	44.5	10	44.5	10
AT5G46960.1	Plant invertase/pectin methylesterase inhibitor					14.94	2	14.94	2
AT5G51750.1	Subtilase 1.3	10.13	5			10.26	5	8.21	4
AT5G59090.2	Subtilase 4.12	23.94	14	25.31	15	12.45	7	14.09	8
AT5G62350.1	Plant invertase/pectin methylesterase inhibitor					11.39	2		
AT5G67360.1	Subtilase family protein	24.7	15	23.65	14	41.61	20	23.65	14

B

		Col		WS	
		% coverage	Nb peptides	% coverage	Nb peptides
AT1G30600.1	Subtilase family protein			8.65	4
AT1G32940.1	Subtilase family protein	20.8	14		
AT1G53830.1	Pectin methylesterase 2	18.91	5	16.87	4
AT2G04160.1	Subtilisin-like serine endopeptidase	15.16	9	18.39	11
AT2G05920.1	Subtilase family protein	62.2	29	62.2	30
AT2G45220.1	Plant invertase/pectin methylesterase inhibitor	30.53	13	31.12	13
AT3G14067.1	Subtilase family protein	38.87	17	38.35	17
AT3G14310.1	Pectin methylesterase 3	23.99	8	19.93	7
AT3G16850.1	Pectin lyase-like superfamily protein	18.46	5	17.58	5
AT3G43270.1	Plant invertase/pectin methylesterase inhibitor			11.2	3
AT3G57790.1	Pectin lyase-like superfamily protein			14.69	7
AT4G19410.1	Pectinacetylesterase family protein	63.94	14	47.39	14
AT4G20430.2	Subtilase family protein	4.21	2	4.21	2
AT4G21650.1	Subtilase family protein			11.1	6
AT4G23500.1	Pectin lyase-like superfamily protein	4.65	2	12.53	4
AT4G25260.1	Plant invertase/pectin methylesterase inhibitor			11.94	2
AT4G33220.1	pectin methylesterase 44			13.9	3
AT4G34980.1	Subtilase family protein	18.85	11	23.04	13
AT5G09760.1	Plant invertase/pectin methylesterase inhibitor	13.43	5	11.8	5
AT5G44530.1	Subtilase family protein	13.81	7	9.05	4
AT5G45280.2	Pectinacetylesterase family protein	47.83	10	43.22	10
AT5G59090.2	Subtilase 4.12	30.23	16	35.15	21
AT5G62350.1	Plant invertase/pectin methylesterase inhibitor			36.63	4
AT5G67360.1	Subtilase family protein	32.76	17	42.8	21

Table I: Identification of homogalacturonan remodeling enzymes and regulators in cell wall-enriched protein extracts of **(A)** 4 day-old dark-grown hypocotyls of wild type Col-0/WS and *pme2* mutants and **(B)** Col-0/WS roots.

Parsed Citations

Andres-Robin, A., Reymond, M.C., Dupire, A., et al. (2018) Evidence for the regulation of gynoecium morphogenesis by ETTIN via cell wall dynamics. Plant Physiol., 178, 1222–1232.
Google Scholar: Author Only Title Only Author and Title

Bader, O., Krauke, Y. and Hube, B. (2008) Processing of predicted substrates of fungal Kex2 proteinases from Candida albicans, C. glabrata, Saccharomyces cerevisiae and Pichia pastoris. BMC Microbiol., 8, 116. Available at: http://bmcmicrobiol.biomedcentral.com/articles/10.1186/1471-2180-8-116 [Accessed June 11, 2020].
Google Scholar: Author Only Title Only Author and Title

Baker, N.A., Sept, D., Joseph, S., Holst, M.J. and McCammon, J.A. (2001) Electrostatics of nanosystems: Application to microtubules and the ribosome. Proc. Natl. Acad. Sci. U. S. A., 98, 10037–10041. Available at: https://pubmed.ncbi.nlm.nih.gov/11517324/ [Accessed November 24, 2020].
Google Scholar: Author Only Title Only Author and Title

Blomberg, N., Gabdoulline, R.R., Nilges, M. and Wade, R.C. (1999) Classification of protein sequences by homology modeling and quantitative analysis of electrostatic similarity. Proteins Struct. Funct. Genet., 37, 379–387. Available at: https://onlinelibrary.wiley.com/doi/full/10.1002/%28SICI%291097-0134%2819991115%2937%3A3%3C379%3A%3AAID-PROT6%3E3.0.CO%3B2-K [Accessed November 17, 2020].
Google Scholar: Author Only Title Only Author and Title

Bosch, M. (2005) Pectin Methylesterases and Pectin Dynamics in Pollen Tubes. Plant Cell Online, 17, 3219–3226. Available at: http://www.plantcell.org/cgi/doi/10.1105/tpc.105.037473.
Google Scholar: Author Only Title Only Author and Title

Bosch, M. and Hepler, P.K. (2005) Pectin methylesterases and pectin dynamics in pollen tubes. Plant Cell, 17, 3219–3226.
Google Scholar: Author Only Title Only Author and Title

Brady, S.M., Orlando, D.A., Lee, J.Y., Wang, J.Y., Koch, J., Dinneny, J.R., Mace, D., Ohler, U. and Benfey, P.N. (2007) A high-resolution root spatiotemporal map reveals dominant expression patterns. Science (80-.)., 318, 801–806.
Google Scholar: Author Only Title Only Author and Title

Braybrook, S.A. and Peaucelle, A. (2013) Mechano-chemical aspects of organ formation in Arabidopsis thaliana: the relationship between auxin and pectin. PLoS One, 8, e57813–e57813. Available at: https://pubmed.ncbi.nlm.nih.gov/23554870.
Google Scholar: Author Only Title Only Author and Title

Cameron, R.G., Luzio, G.A., Goodner, K. and Williams, M.A.K. (2008) Demethylation of a model homogalacturonan with a salt-independent pectin methylesterase from citrus: I. Effect of pH on demethylated block size, block number and enzyme mode of action. Carbohydr. Polym., 71, 287–299. Available at: http://www.sciencedirect.com/science/article/pii/S0144861707003530.
Google Scholar: Author Only Title Only Author and Title

Catoire, L., Pierron, M., Morvan, C., Hervé Du Penhoat, C. and Goldberg, R.E. (1998) Investigation of the Action Patterns of Pectinmethylesterase Isoforms through Kinetic Analyses and NMR Spectroscopy IMPLICATIONS IN CELL WALL EXPANSION*, Available at: http://www.jbc.org/ [Accessed January 6, 2020].

Cheong, M.S., Lee, D.Y., Seo, K.H., Choi, G.H., Song, Y.H., Park, K.H. and Kim, J.H. (2019) Phenylephrine, a small molecule, inhibits pectin methylesterases. Biochem. Biophys. Res. Commun., 508, 320–325.
Google Scholar: Author Only Title Only Author and Title

Daher, F.B., Chen, Y., Bozorg, B., Clough, J., Jönsson, H. and Braybrook, S.A. (2018) Anisotropic growth is achieved through the additive mechanical effect of material anisotropy and elastic asymmetry. Elife, 7. Available at: https://elifesciences.org/articles/38161 [Accessed February 4, 2019].
Google Scholar: Author Only Title Only Author and Title

Dedeurwaerder, S., Menu-Bouaouiche, L., Mareck, A., Lerouge, P. and Guerineau, F. (2009) Activity of an atypical Arabidopsis thaliana pectin methylesterase. Planta, 229, 311–321.
Google Scholar: Author Only Title Only Author and Title

Denès, J.M., Baron, A., Renard, C.M.G.C., Péan, C. and Drilleau, J.F. (2000) Different action patterns for apple pectin methylesterase at pH 7.0 and 4.5. Carbohydr. Res., 327, 385–93. Available at: http://www.ncbi.nlm.nih.gov/pubmed/10990023 [Accessed January 6, 2020].
Google Scholar: Author Only Title Only Author and Title

Dixit, S., Upadhyay, S.K., Singh, H., Pandey, B., Chandrashekar, K. and Verma, P.C. (2013) Pectin methylesterase of Datura species, purification, and characterization from Datura stramonium and its application. Plant Signal. Behav., 8.
Google Scholar: Author Only Title Only Author and Title

Dolinsky, T.J., Nielsen, J.E., McCammon, J.A. and Baker, N.A. (2004) PDB2PQR: An automated pipeline for the setup of Poisson-Boltzmann electrostatics calculations. Nucleic Acids Res., 32. Available at: https://pubmed.ncbi.nlm.nih.gov/15215472/ [Accessed November 24, 2020].
Google Scholar: Author Only Title Only Author and Title

Dorokhov, Y.L., Skurat, E. V., Frolova, O.Y., et al. (2006) Role of the leader sequence in tobacco pectin methylesterase secretion. FEBS Lett., 580, 3329–3334. Available at: http://doi.wiley.com/10.1016/j.febslet.2006.04.090 [Accessed June 11, 2020].
Google Scholar: Author Only Title Only Author and Title

Downie, B., Dirk, L.M.A., Hadfield, K.A., Wilkins, T.A., Bennett, A.B. and Bradford, K.J. (1998) A gel diffusion assay for quantification of pectin methylesterase activity. Anal. Biochem., 264, 149–157.
Google Scholar: Author Only Title Only Author and Title

Duvetter, T., Fraeye, I., Sila, D.N., Verlent, I., Smout, C., Hendrickx, M. and Loey, A. Van (2006) Mode of De-esterification of Alkaline and Acidic Pectin Methyl Esterases at Different pH Conditions. J. Agric. Food Chem., 54, 7825–7831. Available at: https://doi.org/10.1021/jf060013h.
Google Scholar: Author Only Title Only Author and Title

Fendrych, M., Leung, J. and Friml, J. (2016) TIR1/AFB-Aux/IAA auxin perception mediates rapid cell wall acidification and growth of Arabidopsis hypocotyls. Elife, 5, e19048. Available at: https://pubmed.ncbi.nlm.nih.gov/27627746.
Google Scholar: Author Only Title Only Author and Title

Francoz, E., Ranocha, P., Ru, A. Le, Martinez, Y., Fourquaux, I., Jauneau, A., Dunand, C. and Burlat, V. (2019) Pectin Demethylesterification Generates Platforms that Anchor Peroxidases to Remodel Plant Cell Wall Domains. Dev. Cell, 48, 261-276.e8.
Google Scholar: Author Only Title Only Author and Title

Fries, M., Ihrig, J., Brocklehurst, K., Shevchik, V.E. and Pickersgill, R.W. (2007) Molecular basis of the activity of the phytopathogen pectin methylesterase. EMBO J., 26, 3879–3887. Available at: http://emboj.embopress.org/cgi/doi/10.1038/sj.emboj.7601816 [Accessed June 5, 2020].
Google Scholar: Author Only Title Only Author and Title

Goldberg, R., Morvan, C., Jauneau, A. and Jarvis, M.C. (1996) Methyl-esterification, de-esterification and gelation of pectins in the primary cell wall. Prog. Biotechnol., 14, 151–172.
Google Scholar: Author Only Title Only Author and Title

Hervé, V., Duruflé, H., San Clemente, H., Albenne, C., Balliau, T., Zivy, M., Dunand, C. and Jamet, E. (2016) An enlarged cell wall proteome of Arabidopsis thaliana rosettes. Proteomics, 16, 3183–3187. Available at: http://doi.wiley.com/10.1002/pmic.201600290 [Accessed June 11, 2020].
Google Scholar: Author Only Title Only Author and Title

Hewezi, T., Howe, P., Maier, T.R., Hussey, R.S., Mitchum, M.G., Davis, E.L. and Baum, T.J. (2008) Cellulose binding protein from the parasitic nematode Heterodera schachtii interacts with Arabidopsis pectin methylesterase: cooperative cell wall modification during parasitism. Plant Cell, 20, 3080–93. Available at: http://www.ncbi.nlm.nih.gov/pubmed/19001564 [Accessed February 5, 2019].
Google Scholar: Author Only Title Only Author and Title

Hocq, L., Guinand, S., Habrylo, O., et al. (2020) The exogenous application of AtPGLR, an endo-polygalacturonase, triggers pollen tube burst and repair. Plant J., n/a. Available at: https://doi.org/10.1111/tpj.14753.
Google Scholar: Author Only Title Only Author and Title

Hocq, L., Pelloux, J. and Lefebvre, V. (2017) Connecting Homogalacturonan-Type Pectin Remodeling to Acid Growth. Trends Plant Sci., 22, 20–29. Available at: http://dx.doi.org/10.1016/j.tplants.2016.10.009.
Google Scholar: Author Only Title Only Author and Title

Hocq, L., Sénéchal, F., Lefebvre, V., et al. (2017) Combined Experimental and Computational Approaches Reveal Distinct pH Dependence of Pectin Methylesterase Inhibitors. Plant Physiol., 173, 1075–1093. Available at: http://www.plantphysiol.org/lookup/doi/10.1104/pp.16.01790.
Google Scholar: Author Only Title Only Author and Title

Hruz, T., Laule, O., Szabo, G., Wessendorp, F., Bleuler, S., Oertle, L., Widmayer, P., Gruissem, W. and Zimmermann, P. (2008) Genevestigator V3: A Reference Expression Database for the Meta-Analysis of Transcriptomes Y. Van de Peer, ed. Adv. Bioinformatics, 2008, 420747. Available at: https://doi.org/10.1155/2008/420747.
Google Scholar: Author Only Title Only Author and Title

Johansson, K., El-Ahmad, M., Friemann, R., Jörnvall, H., Markovič, O. and Eklund, H. (2002) Crystal structure of plant pectin methylesterase. FEBS Lett., 514, 243–249.
Google Scholar: Author Only Title Only Author and Title

Jolie, R.P., Duvetter, T., Loey, A.M. Van and Hendrickx, M.E. (2010) Pectin methylesterase and its proteinaceous inhibitor: A review. Carbohydr. Res., 345, 2583–2595.
Google Scholar: Author Only Title Only Author and Title

Kent, L.M., Loo, T.S., Melton, L.D., Mercadante, D., Williams, M.A.K. and Jameson, G.B. (2016) Structure and properties of a non-processive, salt-requiring, and acidophilic pectin methylesterase from aspergillus Niger provide insights into the key determinants of processivity control. J. Biol. Chem., 291, 1289–1306.
Google Scholar: Author Only Title Only Author and Title

Kumpf, R.P., Shi, C.-L., Larrieu, A., Sto, I.M., Butenko, M.A., Peret, B., Riiser, E.S., Bennett, M.J. and Aalen, R.B. (2013) Floral organ abscission peptide IDA and its HAE/HSL2 receptors control cell separation during lateral root emergence. Proc. Natl. Acad. Sci., 110,

5235–5240. Available at: http://www.pnas.org/cgi/doi/10.1073/pnas.1210835110.
Google Scholar: Author Only Title Only Author and Title

Leroux, C., Bouton, S., Kiefer-Meyer, M.-C., et al. (2015) PECTIN METHYLESTERASE48 Is Involved in Arabidopsis Pollen Grain Germination. Plant Physiol., 167, 367–380. Available at: http://www.plantphysiol.org/lookup/doi/10.1104/pp.114.250928.
Google Scholar: Author Only Title Only Author and Title

Lin, T.-P., Liu, C.-C., Chen, S.-W. and Wang, W.-Y. (1989) Purification and Characterization of Pectinmethylesterase from Ficus awkeotsang Makino Achenes . Plant Physiol., 91, 1445–1453.
Google Scholar: Author Only Title Only Author and Title

Malamy, J.E. and Benfey, P.N. (1997) . , 44, 33–44.
Google Scholar: Author Only Title Only Author and Title

Markovič, O. and Janeček, Š. (2004) Pectin methylesterases: Sequence-structural features and phylogenetic relationships. Carbohydr. Res., 339, 2281–2295.
Google Scholar: Author Only Title Only Author and Title

Markovič, O. and Kohn, R. (1984) Mode of pectin deesterification by Trichoderma reesei pectinesterase. Experientia, 40, 842–843.
Google Scholar: Author Only Title Only Author and Title

Mercadante, D., Melton, L.D., Jameson, G.B. and Williams, M.A.K. (2014) Processive pectin methylesterases: the role of electrostatic potential, breathing motions and bond cleavage in the rectification of Brownian motions. PLoS One, 9, e87581. Available at: http://www.ncbi.nlm.nih.gov/pubmed/24503943 [Accessed June 5, 2020].
Google Scholar: Author Only Title Only Author and Title

Mercadante, D., Melton, L.D., Jameson, G.B., Williams, M.A.K. and Simone, A. De (2013) Substrate dynamics in enzyme action: Rotations of monosaccharide subunits in the binding groove are essential for pectin methylesterase processivity. Biophys. J., 104, 1731–1739. Available at: http://dx.doi.org/10.1016/j.bpj.2013.02.049.
Google Scholar: Author Only Title Only Author and Title

Micheli, F. (2001) Pectin methylesterases: Cell wall enzymes with important roles in plant physiology. Trends Plant Sci., 6, 414–419.
Google Scholar: Author Only Title Only Author and Title

Milani, P., Gholamirad, M., Traas, J., Arnéodo, A., Boudaoud, A., Argoul, F. and Hamant, O. (2011) In vivo analysis of local wall stiffness at the shoot apical meristem in Arabidopsis using atomic force microscopy. Plant J., 67, 1116–1123.
Google Scholar: Author Only Title Only Author and Title

Nguyen-Kim, H., San Clemente, H., Balliau, T., Zivy, M., Dunand, C., Albenne, C. and Jamet, E. (2016) Arabidopsis thaliana root cell wall proteomics: Increasing the proteome coverage using a combinatorial peptide ligand library and description of unexpected Hyp in peroxidase amino acid sequences. Proteomics, 16, 491–503. Available at: http://doi.wiley.com/10.1002/pmic.201500129 [Accessed May 22, 2019].
Google Scholar: Author Only Title Only Author and Title

Peaucelle, A., Braybrook, S.A., Le Guillou, L., Bron, E., Kuhlemeier, C. and Höfte, H. (2011) Pectin-Induced Changes in Cell Wall Mechanics Underlie Organ Initiation in Arabidopsis. Curr. Biol., 21, 1720–1726. Available at: http://www.sciencedirect.com/science/article/pii/S0960982211009638.
Google Scholar: Author Only Title Only Author and Title

Peaucelle, A., Louvet, R., Johansen, J.N., et al. (2011) The transcription factor BELLRINGER modulates phyllotaxis by regulating the expression of a pectin methylesterase in Arabidopsis. Development, 138, 4733–4741.
Google Scholar: Author Only Title Only Author and Title

Peaucelle, A., Louvet, R., Johansen, J.N., Höfte, H., Laufs, P., Pelloux, J. and Mouille, G. (2008) Arabidopsis phyllotaxis is controlled by the methyl-esterification status of cell-wall pectins. Curr. Biol., 18, 1943–8. Available at: http://www.ncbi.nlm.nih.gov/pubmed/19097903.
Google Scholar: Author Only Title Only Author and Title

Peaucelle, A., Wightman, R. and Höfte, H. (2015) The Control of Growth Symmetry Breaking in the Arabidopsis Hypocotyl. Curr. Biol., 25, 1746–1752.
Google Scholar: Author Only Title Only Author and Title

Pelletier, S., Orden, J. Van, Wolf, S., et al. (2010) A role for pectin de-methylesterification in a developmentally regulated growth acceleration in dark-grown Arabidopsis hypocotyls. New Phytol., 188, 726–739.
Google Scholar: Author Only Title Only Author and Title

Pelloux, J., Rustérucci, C. and Mellerowicz, E.J. (2007) New insights into pectin methylesterase structure and function. Trends Plant Sci., 12, 267–277.
Google Scholar: Author Only Title Only Author and Title

Peng, C.C., Hsiao, E.S.L., Ding, J.L.C. and Tzen, J.T.C. (2005) Functional expression in Pichia pastoris of an acidic pectin methylesterase from jelly fig (Ficus awkeotsang). J. Agric. Food Chem., 53, 5612–5616.
Google Scholar: Author Only Title Only Author and Title

Refrégier, G., Pelletier, S., Jaillard, D. and Höfte, H. (2004) Interaction between wall deposition and cell elongation in dark-grown

hypocotyl cells in Arabidopsis. Plant Physiol., 135, 959–968.
Google Scholar: Author Only Title Only Author and Title

Ren, C. and Kermode, A.R. (2000) An increase in pectin methyl esterase activity accompanies dormancy breakage and germination of yellow cedar seeds. Plant Physiol., 124, 231–242. Available at: /pmc/articles/PMC59138/?report=abstract [Accessed June 30, 2020].
Google Scholar: Author Only Title Only Author and Title

Ridley, B.L., O'Neill, M.A. and Mohnen, D. (2001) Pectins: Structure, biosynthesis, and oligogalacturonide-related signaling. Phytochemistry, 57, 929–967. Available at: https://pubmed.ncbi.nlm.nih.gov/11423142/ [Accessed November 5, 2020].
Google Scholar: Author Only Title Only Author and Title

Salamin, K., Sriranganadane, D., Léchenne, B. and Jousson, O. (2010) Endogenous Secreted Subtilisin in Pichia pastoris GS115 and KM71 Strains 1 2. Available at: http://aem.asm.org/ [Accessed June 11, 2020].
Google Scholar: Author Only Title Only Author and Title

San Clemente, H. and Jamet, E. (2015) WallProtDB, a database resource for plant cell wall proteomics. Plant Methods, 11, 1–7.
Google Scholar: Author Only Title Only Author and Title

Savary, B.J. (2001) Perfusion chromatography separation of the tomato fruit-specific pectin methylesterase from a semipurified commercial enzyme preparation. Prep. Biochem. Biotechnol., 31, 241–258.
Google Scholar: Author Only Title Only Author and Title

Savary, B.J., Vasu, P., Cameron, R.G., McCollum, T.G. and Nuñez, A. (2013) Structural Characterization of the Thermally Tolerant Pectin Methylesterase Purified from Citrus sinensis Fruit and Its Gene Sequence. J. Agric. Food Chem., 61, 12711–12719. Available at: https://doi.org/10.1021/jf403914u.
Google Scholar: Author Only Title Only Author and Title

Savary, B.J., Vasu, P., Nunez, A. and Cameron, R.G. (2010) Identification of thermolabile pectin methylesterases from sweet orange fruit by peptide mass fingerprinting. J. Agric. Food Chem., 58, 12462–12468.
Google Scholar: Author Only Title Only Author and Title

Sénéchal, F., Graff, L., Surcouf, O., et al. (2014) Arabidopsis PECTIN METHYLESTERASE17 is co-expressed with and processed by SBT3.5, a subtilisin-like serine protease. Ann. Bot., 114, 1161–1175.
Google Scholar: Author Only Title Only Author and Title

Sénéchal, F., L'Enfant, M., Domon, J.M., et al. (2015) Tuning of pectin methylesterification: Pectin methylesterase inhibitor 7 modulates the processive activity of co-expressed pectin methylesterase 3 in a pH-dependentmanner. J. Biol. Chem., 290, 23320–23335.
Google Scholar: Author Only Title Only Author and Title

Sénéchal, F., Wattier, C., Rustérucci, C. and Pelloux, J. (2014) Homogalacturonan-modifying enzymes: Structure, expression, and roles in plants. J. Exp. Bot., 65, 5125–5160.
Google Scholar: Author Only Title Only Author and Title

Søndergaard, C.R., Olsson, M.H.M., Rostkowski, M. and Jensen, J.H. (2011) Improved treatment of ligands and coupling effects in empirical calculation and rationalization of p K a values. J. Chem. Theory Comput., 7, 2284–2295. Available at: https://pubmed.ncbi.nlm.nih.gov/26606496/ [Accessed November 24, 2020].
Google Scholar: Author Only Title Only Author and Title

Swarup, K., Benková, E., Swarup, R., et al. (2008) The auxin influx carrier LAX3 promotes lateral root emergence. Nat. Cell Biol., 10, 946–954.
Google Scholar: Author Only Title Only Author and Title

Thonar, C., Liners, F. and Cutsem, P. Van (2006) Polymorphism and modulation of cell wall esterase enzyme activities in the chicory root during the growing season. J. Exp. Bot., 57, 81–89. Available at: http://academic.oup.com/jxb/article/57/1/81/442028/Polymorphism-and-modulation-of-cell-wall-esterase [Accessed January 6, 2020].
Google Scholar: Author Only Title Only Author and Title

Voxeur, A., Habrylo, O., Guénin, S., et al. (2019) Oligogalacturonide production upon Arabidopsis thaliana-Botrytis cinerea interaction. Proc. Natl. Acad. Sci. U. S. A., 116, 19743–19752.
Google Scholar: Author Only Title Only Author and Title

Wachsman, G., Zhang, J., Moreno-Risueno, M.A., Anderson, C.T. and Benfey, P.N. (2020) Cell wall remodeling and vesicle trafficking mediate the root clock in Arabidopsis. Science, 370, 819–823.
Google Scholar: Author Only Title Only Author and Title

Wade, R.C., Gabdoulline, R.R. and Rienzo, F. De (2001) Protein interaction property similarity analysis. Int. J. Quantum Chem., 83, 122–127. Available at: http://doi.wiley.com/10.1002/qua.1204 [Accessed November 17, 2020].
Google Scholar: Author Only Title Only Author and Title

Wang, J., Cieplak, P. and Kollman, P.A. (2000) How Well Does a Restrained Electrostatic Potential (RESP) Model Perform in Calculating Conformational Energies of Organic and Biological Molecules? Keywords: additive force field; nonadditive force field; restrained electrostatic potential (RESP); torsional angle parameterization, Available at: www.amber.ucsf.edu/amber/ [Accessed November 24, 2020].

Wang, X., Wilson, L. and Cosgrove, D.J. (2020) Pectin methylesterase selectively softens the onion epidermal wall yet reduces acid-induced creep. J. Exp. Bot., 71, 2629–2640. Available at: https://pubmed.ncbi.nlm.nih.gov/32006044.
Google Scholar: Author Only Title Only Author and Title

Willats, W.G.T., Knox, J.P. and Mikkelsen, J.D. (2006) Pectin: New insights into an old polymer are starting to gel. Trends Food Sci. Technol., 17, 97–104.
Google Scholar: Author Only Title Only Author and Title

Willats, W.G.T., Orfila, C., Limberg, G., et al. (2001) Modulation of the degree and pattern of methyl-esterification of pectic homogalacturonan in plant cell walls: Implications for pectin methyl esterase action, matrix properties, and cell adhesion. J. Biol. Chem., 276, 19404–19413.
Google Scholar: Author Only Title Only Author and Title

Wolf, S., Rausch, T. and Greiner, S. (2009) The N-terminal pro region mediates retention of unprocessed type-I PME in the Golgi apparatus. Plant J., 58, 361–375.
Google Scholar: Author Only Title Only Author and Title